RESEARCH MEMORANDUM

AN INVESTIGATION OF CONVERGENT-DIVERGENT DIFFUSERS AT MACH NUMBER 1.85

By DeMarquis D. Wyatt and Henry R. Hunczak

Lewis Flight Propulsion Laboratory
Cleveland, Ohio

NATIONAL ADVISORY COMMITTEE
FOR AERONAUTICS

WASHINGTON
February 2, 1951

NACA RM E50L07

NATIONAL ADVISORY COMMITTEE FOR AERONAUTICS

RESEARCH MEMORANDUM

AN INVESTIGATION OF CONVERGENT-DIVERGENT DIFFUSERS AT MACH NUMBER 1.85

By DeMarquis D. Wyatt and Henry R. Hunczak

SUMMARY

An investigation was conducted in the NACA Lewis 18- by 18-inch supersonic tunnel at a Mach number of 1.85 and angles of attack from 0° to 5° to determine optimum design configurations for a convergent-divergent type of supersonic diffuser with a subsonic diffuser of 5° included divergence angle. Total-pressure recoveries in excess of theoretical recovery across a normal shock at a free-stream Mach number of 1.85 were obtained with several configurations.

The highest recovery for configurations without a cylindrical throat section was obtained with an inlet having an included convergence angle of 20°. Insertion of a 2-inch throat section between a 10° included angle inlet and the subsonic diffuser stabilized the shock inside the diffuser and resulted in recoveries as high as 0.838 free-stream total pressure at an angle of attack of 0°, corresponding to recovery of 92.4 percent of the kinetic energy of the free air stream. Use of the throat section also lessened the reduction in recovery of all configurations due to angle of attack.

INTRODUCTION

Diffusion of the free air stream in a manner that results in maximum total-pressure recovery is essential to efficient operation of ram-jet engines. The particular necessity for determining the optimum diffuser designs for supersonic ram-jet engines is accentuated by the losses in total pressure associated with normal shock waves. The effect of the shock can be minimized only through reduction of the Mach number at which the shock occurs. Diffusers that accomplish this desired reduction in Mach number have been proposed by Oswatitsch (reference 1) and Kantrowitz and Donaldson (reference 2).

Reference 2 presents the theory of the convergent-divergent diffuser together with preliminary experimental results of such a diffuser at an angle of attack of 0°.

As part of a general study of supersonic diffusers, a detailed program has been undertaken at the NACA Lewis laboratory to establish optimum design configurations for the convergent-divergent type of supersonic diffuser. Data have been obtained in the 18- by 18-inch supersonic tunnel at a Mach number of 1.85 to show the effects of inlet angle and straight throat length after contraction on the pressure recovery at angles of attack up to 5°. The results include the effect of variations of the outelt flow area of the diffusers. Data are also presented for a diffuser having a cylindrical inlet with no contraction and for a simple diverging diffuser to serve as a comparative basis for evaluating the convergent-divergent type of diffuser.

APPARATUS AND PROCEDURE

The diffuser combinations were tested in the Lewis 18- by 18-inch supersonic tunnel, which at the time was calibrated by measuring the angle of an oblique shock generated by a cone. This method is accurate to about 2 percent in determining the free-stream Mach number at the diffuser inlet.

The complete test configuration consisted of a cylindrical section simulating a ram-jet combustion chamber, a straight tapered subsonic diffuser with an included divergence angle of 5°, and straight tapered inlets and cylindrical throat sections fitted on the subsonic diffuser in the desired combinations. The schematic arrangement and principal dimensions of the model are given in figure 1. No fairing was used at any of the junctures between the component parts.

The investigation included tests of 10 convergent, 1 cylindrical, and 1 divergent inlet (fig. 1) alone and in combination with various-length throats. The principal dimensions of the inlets and a summary of the inlet-throat combinations investigated are given in table I.

The inlet-throat combinations using convergent inlets are identified in table I and will be referred to in the rest of the report according to the following practice: The first numeral indicates the included convergence angle of the inlet τ, the second numeral gives the geometrical contraction ratio of the inlet (nose area/minimum area), and the third numeral shows the length of straight throat section L. (See fig. 1.) For example, configuration 5-1.190-0 denotes an inlet with $\tau = 5°$ and a contraction ratio of 1.190 used without a throat section.

The locations of pitot tubes, static-pressure orifices, and pitot-static tubes used in determining the pressure conditions at the entrance to the simulated combustion chamber are shown in figure 2. Additional static orifices were located in the inlets, the throats, and the subsonic diffuser for determining the longitudinal static-pressure distribution. The pressure tubes connected to these orifices were carried along the outside surface of the diffuser without external fairing.

Total pressures in the free stream at the diffuser inlets were calculated from total pressures measured in the tunnel settling chamber. The ratio of free-stream total pressure to settling-chamber total pressure had been established for each inlet position from a previous tunnel calibration and these ratios were assumed to be constant throughout the tests.

All pressures were photographically recorded on a multiple-tube mercury manometer. Air-flow conditions about the diffuser inlet were observed with a two-mirror schlieren system and were occasionally photographed for record purposes.

Configuration 10-1.176-2 was investigated at angles of attack of 0°, 1°, 3°, and 5°; the other configurations were tested only at 0° and 5°. At each angle of attack the back pressure on the diffuser outlet was changed by varying the outlet area of the simulated combustion chamber by means of a conical plug at the rear of the model. (See fig. 1.)

RESULTS AND DISCUSSION

When the outlet passage of the simulated combustion chamber was closed, an unsteady oscillation of the shock bow wave ahead of the diffuser inlet was visually observed through the schlieren system for all configurations. The typical movement of the shock wave as the outlet passage was opened is shown in figure 3 by the schlieren photographs of the 5-1.190-0 configuration at 5° angle of attack. At small ratios of combustion-chamber-outlet area to diffuser-inlet area (A_5/A_1) the air flow through the model was sufficient to steady the normal shock ahead of the inlet as shown in figure 3(a). The shock directly ahead of the diffuser inlet appears to be normal to the air stream rather than parallel to the diffuser-entrance plane in this photograph. This relative position was observed at all angles of attack. When A_5/A_1 was further increased the normal shock moved toward the inlet (fig. 3(b)) and finally was entirely

contained within the diffuser (fig. 3(c)). Operation at this final shock position is considered desirable with this type of diffuser in order to avoid high external nose pressures and to increase the mass rate of air flow through the diffuser.

Typical static-pressure distributions along the internal walls of the inlet, the throat section, and the subsonic diffuser of the 20-1.190-2 configuration are shown in figure 4 as the ratio of wall static pressure to free-stream total pressure, p/P_0. Progressive motion of the normal shock wave into the inlet and down the subsonic diffuser as the outlet area was increased is apparent from the position of the sharp upward break in the pressure curve at the different conditions. At 5° angle of attack (fig. 4(b)) the pressure differential between the upper and lower surfaces of the diffuser (solid and dashed lines) caused by wave reflections and impact was rapidly damped.

Static-pressure distributions (p/P_0) at the entrance to the combustion chamber for a typical configuration are presented in figure 5. The pressure-tube locations in figure 2 are translated to lie in a single vertical plane in the plotting of figure 5; two pressures are therefore plotted at each point. As expected, the static pressure across the combustion chamber was apparently equalized. The variations in total-pressure recovery (P_4/P_0) shown in figure 6 therefore indicate changes in the velocity distribution across the combustion chamber. Wall static pressures plotted as total pressures at the 1.8-inch-radius position give a means of ready estimation of dynamic pressure. For all configurations the flow was almost uniform through the combustion chamber at all angles of attack for values of A_5/A_1 less than approximately 2.30. A nonuniform velocity distribution occurred at larger values of A_5/A_1. A symmetrical high-velocity region occurred at the center of the combustion chamber at 0° angle of attack. The peak velocity shifted slightly toward the top at 5° angle of attack.

Static pressures measured along the top internal surfaces of the inlet and the forward portion of the subsonic diffuser are presented in figure 7 for the configurations having the 1.190 contraction ratio inlets without throat sections. Supersonic flow was established into the inlets having included convergence angles from 5° to 20° for values of A_5/A_1 greater than approximately 0.9, as shown from the low static pressures in the inlets. The contraction ratio 1.190 used in these inlets was selected prior to calibration of the tunnel on the supposition that the Mach number of the tunnel test section would be 1.89. This contraction ratio would result in over-contraction of the air stream at a Mach number of 1.85 and,

according to one-dimensional theory, the shock would remain outside the inlet. (See reference 2.) The difference between the two Mach numbers, 1.85 and 1.89, is within the precision of the tunnel calibration.

Static pressures in the inlets of the 30-1.190-0 and 40-1.190-0 configurations remained high for all conditions of A_5/A_1, showing that a normal shock occurred ahead of the throat. Visual observation of the inlets through the schlieren system disclosed, however, that the normal shock did not remain ahead of the inlets. It is believed that an inversed bow shock occurred just inside the inlets in a manner theoretically predicted by Ferri (reference 3).

The static pressures in the inlets for conditions where the normal shock had entered are plotted in figure 8 to show the comparison with the theoretical pressure distributions determined from considerations of the flow-turning angle alone. (See reference 4.) In the determination of the theoretical curves it was assumed that the deflection of the flow by the inlet lip was analogous to the deflection caused by flow into a corner equal to half the included convergence angle of the inlet. The location of the measured pressures above the respective theoretical pressures shows a flow compression indicative of transition from two- to three-dimensional flow, approximating the flow field analytically investigated by Ferri.

The total-pressure recoveries (P_4/P_0) of the inlets with 1.190 contraction ratio are presented in figure 9 as a function of A_5/A_1. The theoretical recovery as determined from one-dimensional nonviscous theory based on a choking condition at the combustion-chamber outlet is included. (See the appendix.)

According to theory, the normal shock should have remained outside the diffuser with resultant total-pressure recoveries corresponding to a normal shock at a free-stream Mach number of 1.85 for values of A_5/A_1 less than 0.846. At this area ratio the normal shock should have entered the inlet and reestablished itself in the subsonic diffuser at an upstream Mach number of 1.85. A decrease in combustion-chamber-outlet area to give $A_5/A_1 = 0.751$ should have moved the shock back to the throat where it would occur at the minimum upstream Mach number and give the maximum total-pressure recovery. Conversely, increasing A_5/A_1 above 0.846 should have drawn the shock farther into the diffuser, resulting in higher upstream Mach numbers and resultant reduced pressure recoveries.

Pressure recoveries at very low values of A_5/A_1 approximated theoretical recoveries for a shock at free-stream Mach number inasmuch as the diffuser was essentially operating as a total-head tube under those conditions. As A_5/A_1 was increased the measured recoveries fell below the theoretical recoveries, owing to friction losses in the diffuser. The point of sharp change of curvature of the pressure-recovery curve occurred at values of A_5/A_1 between 0.9 and 1.0 for all inlets, indicating that shock losses first occurred in the subsonic diffuser at those area ratios.

Recoveries with the shock inside the subsonic diffuser showed good agreement in slope with the theoretical curves, but the area ratios A_5/A_1 were larger than the theoretical values. The general shift is attributed to discrepancies between the measured geometrical outlet area A_5 and the ideal flow area upon which the theoretical curves are based. Friction effects contribute to the variations in displacement among the several diffusers.

The peaked recovery curves obtained with inlets of 5°, 10°, 15°, and 20° included convergence angle indicate that the normal shock wave was moved closer to the throat by a decrease in A_5/A_1 after the shock had entered the inlet. The general trend of the data shows increasing values of recovery as the inlet angle was increased. The maximum recovery measured was 0.814 of the free-stream total pressure (fig. 9(d)) and was obtained with the 20-1.190-0 configurations. Recovery curves for the 30-1.190-0 and 40-1.190-0 configurations show no peaks because of the strong inverse bow wave ahead of the throat (reference 3). Operation of the inlets at 5° angle of attack resulted in loss of most or all of the peaked recoveries present at 0° angle of attack but otherwise had no effect on the slope or magnitude of the recovery curves.

The series of inlets designed with a contraction ratio of 1.176 (slightly under the theoretical maximum for a free-stream Mach number of 1.85) gave recovery curves similar to those obtained for the inlets with a contraction ratio of 1.190 but maximum recoveries were slightly lower, as had been theoretically anticipated. (See fig. 10.)

Data obtained from tests of the cylindrical inlet and of the inlet that diverged at an included angle of 5°, thereby forming a continuation of the subsonic diffuser, are presented in figures 11 and 12. No peak in pressure recovery is theoretically possible with either inlet. Comparison of the results from tests of the converging inlets and tests of the cylindrical and diverging inlets show that

the improved total-pressure recoveries of the converging inlets are obtainable only with close control of A_5/A_1. All inlets showed approximately the same characteristics at 5° angle of attack inasmuch as peaked recoveries were largely unobtainable with the convergent inlets.

The maximum recoveries of the several inlets corresponding to conditions with the normal shock inside the diffuser are summarized in figure 13. For these tests without throats the maximum recovery was obtained with the 20-1.190-0 configuration; the maximum recovery exceeded the theoretical recovery behind a normal shock at a free-stream Mach number of 1.85 by 3 percent.

According to a theory of shock-wave stability proposed by Kantrowitz (reference 5), insertion of a straight throat section between the inlet and the subsonic diffuser should result in increased pressure recoveries by decreasing the tendency of the shock to jump ahead of the inlet when an attempt is made to locate it near the minimum section.

Throat sections 1, 2, and 4 inches in length were investigated to validate this theory. Static-pressure distributions in the inlets, the throats, and a portion of the subsonic diffuser for each of the configurations tested are shown in figure 14. Retention of the normal shock wave inside the diffuser as evidenced by inlet static pressures of the order of 0.20 free-stream total pressure occurred at minimum values of A_5/A_1 of 0.931 for the configuration without the throat, 0.906 for the 1-inch throat, and 0.860 for the 2-inch throat, thereby indicating operation of the throats as theoretically anticipated. (See the appendix.)

Supersonic flow was never established into the inlet of the configuration with the 4-inch throat owing to the build-up of boundary layer. The presence of the boundary layer is shown by the decreasing static pressures in the direction of air flow in the throat section.

The pressure recoveries obtained with the configurations used to investigate the effect of throat length are presented in figure 15; the maximum recoveries are plotted in figure 16 as a function of throat length. Insertion of the 1-inch throat resulted in a 4.4-percent increase in maximum pressure recovery as compared with the recovery of the same inlet with no throat and insertion of the 2-inch throat resulted in an 8.2-percent increase. Use of the 4-inch throat section decreased the maximum recovery owing to failure of the normal shock wave to enter the inlet. All configurations gave approximately the same results at 5° angle of attack; a pressure peak was unobtainable.

The results of several inlets tested in combination with the 2-inch throat to determine the possibilities of combining the peak recoveries of the inlets and the throat showed consistently high recoveries with all combinations. (See figs. 17 and 18.) The maximum recovery (fig. 18) was obtained with smaller inlet convergence angles than was the case in the configurations with no throats (fig. 13); the maximum total-pressure recovery of 0.838 free-stream total pressure was obtained with the 10-1.176-2 configuration. The recovery of the 20-1.176-2 configuration was greater than the recovery with the 20-1.190-2 configuration, which was a reversal of the results from the same inlets without throat sections.

The maximum recoveries of the configurations having the 2-inch throat section remained somewhat higher at increasing angles of attack than did the configurations without throats. The maximum recoveries (with the shock swallowed) of the 10-1.176-2 configuration at several angles of attack from 0° to 5° are shown in figure 19 as a function of angle of attack.

The summarized data of figures 13, 15, and 18 are presented in figures 20 and 21 in terms of the energy efficiency of the diffuser. The energy efficiency η is defined as the portion of available kinetic energy in the free air stream that is recovered in the diffusion process. The equation for this value in terms of the total pressures in the free stream and at the diffuser outlet is developed in reference 2 and, in the notation of the present paper, is:

$$\eta = 1 - \frac{5}{M_0^2}\left[\left(\frac{P_0}{P_4}\right)^{\frac{1}{3.5}} - 1\right]$$

where P_0 and P_4 are the total pressures in the free stream and at the diffuser outlet, respectively, and M_0 is the free-stream Mach number.

The maximum efficiency for the configurations without throat sections was obtained with the 20-1.190-0 configuration; 91.2 percent of the kinetic energy of the free air stream was recovered. Addition of the 2-inch throat resulted in a maximum efficiency of 92.4 percent for the 10-1.176-2 configuration.

SUMMARY OF RESULTS

As part of a general study of supersonic diffusers, an investigation of several inlet and throat combinations tested at a free-stream Mach number of 1.85 in a convergent-divergent diffuser arrangement with a subsonic diffuser of 5° included divergence angle gave the following results:

1. Total-pressure recoveries in excess of the theoretical recovery across a normal shock at a free-stream Mach number of 1.85 were obtained with a number of configurations. The maximum total-pressure recovery was obtained with an inlet having a contraction ratio of 1.176 and an included convergence angle of 10° operated in combination with a 2-inch straight throat section between the inlet and the subsonic diffuser. The throat was found to stabilize the shock inside the diffuser. The maximum pressure recovery at 0° angle of attack with this configuration was 0.838 free-stream total pressure and corresponded to recovery of 92.4 percent of the kinetic energy of the free air stream.

2. Configurations tested without throat sections gave highest recoveries with an inlet having an included convergence angle of 20°. Inlets having a contraction ratio of 1.190 gave slightly higher recoveries than corresponding inlets of 1.176 contraction ratio.

3. Operations of configurations at 5° angle of attack resulted in reduction of the maximum total-pressure recoveries obtained with the shock inside the diffuser to below the theoretical recovery behind a shock at free-stream Mach number. The use of a 2-inch throat section lessened the reduction in recovery due to angle of attack.

4. The velocity distribution at the outlet of the subsonic diffuser was found to be reasonably uniform for all configurations at ratios of combustion-chamber-outlet area to diffuser-inlet area required to maintain the normal shock near the throat of the diffuser.

Lewis Flight Propulsion Laboratory,
National Advisory Committee for Aeronautics,
Cleveland, Ohio.

APPENDIX - CALCULATION OF THEORETICAL TOTAL-PRESSURE RECOVERY AS A FUNCTION OF THE RATIO OF COMBUSTION-CHAMBER-OUTLET AREA TO DIFFUSER-INLET AREA

The theoretical total-pressure-recovery curves in figures 9 to 12 and figures 15 and 17 were based on an assumed one-dimensional nonviscous air flow according to the following analysis:

It can be shown that the equation $m = \rho VA$ for the mass rate of air flow m through a closed channel can be rewritten in terms of the Mach number M as

$$m = \sqrt{\frac{\gamma}{RT}}\, PAM \left(1 + \frac{\gamma-1}{2} M^2\right)^{-\frac{\gamma+1}{2(\gamma-1)}} \qquad (2)$$

where

m mass rate of air flow

ρ density

V velocity

A flow area

γ ratio of specific heat at constant pressure to specific heat at constant volume

R gas constant

T stagnation temperature

P total pressure

M Mach number

If the air flowing through the diffuser enters with free-stream velocity (that is, the shock is swallowed), the mass flow is constant irrespective of outlet conditions and may be determined from conditions of any point in the system. If flow through the diffuser and

the simulated combustion chamber without heat transfer is assumed, the stagnation temperature of the air is unchanged. From conservation of mass, the relation between the total pressure and the flow area at the inlet to the diffuser and at the outlet of the simulated combustion chamber can therefore be derived from equation (2) as

$$\left(\frac{A_5}{A_1}\right)\left(\frac{P_5}{P_1}\right) = \frac{M_1}{M_5}\left(\frac{1 + \frac{\gamma-1}{2} M_5^2}{1 + \frac{\gamma-1}{2} M_1^2}\right)^{\frac{\gamma+1}{2(\gamma-1)}} \tag{3}$$

where subscripts 1 and 5 denote conditions at the diffuser inlet and the simulated combustion-chamber outlet, respectively.

The total pressure at the diffuser outlet P_4 can be substituted for P_5 by assuming frictionless flow; P_1 can be replaced by the free-stream total pressure P_0; and M_1 can be replaced by the free-stream Mach number M_0 because the shock is assumed to occur inside the diffuser. Sonic velocity occurs at the combustion-chamber outlet and M_5 has a value of 1.0. Therefore equation (3) reduces to the form,

$$\left(\frac{A_5}{A_1}\right)\left(\frac{P_4}{P_0}\right) = M_0\left(\frac{1 + \frac{\gamma-1}{2}}{1 + \frac{\gamma-1}{2} M_0^2}\right)^{\frac{\gamma+1}{2(\gamma-1)}} \tag{4}$$

The right-hand member of equation (4) is the reciprocal of the isentropic area ratio required to accelerate the air from sonic velocity to Mach number M_0 and is a constant for any given flight Mach number. At Mach number 1.85 the value of the constant is 0.669 ($\gamma = 1.400$).

The highest recovery for which equation (4) is valid is the recovery across a normal shock located at the throat of the diffuser. This value must be determined from one-dimensional calculations applied to the given configuration. The area ratio A_5/A_1 thereby determined is the minimum for retention of the normal shock inside the diffuser. Any further reduction in A_5/A_1 forces the normal shock wave ahead of the diffuser, where it occurs at free-stream Mach number, and the total-pressure recovery remains constant at the free-stream shock-recovery value.

An increase in A_5/A_1 moves the normal shock downstream from the throat of the diffuser and decreases the total-pressure recovery according to equation (4) as the shock occurs at progressively higher Mach numbers.

The minimum pressure recovery satisfying the conditions of equation (4) is the value that gives sonic velocity at the combustion-chamber outlet with a static pressure just equal to the free-stream static pressure. This minimum total-pressure recovery is independent of the configuration and is given by the formula

$$\left(\frac{P_4}{P_0}\right)_{min.} = \left(\frac{1 + \frac{\gamma-1}{2}}{1 + \frac{\gamma-1}{2} M_0^2}\right)^{\frac{\gamma}{\gamma-1}} \qquad (5)$$

REFERENCES

1. Oswatitsch, Kl.: Der Druckrückgewinn bei Geschossen mit Rückstossantrieb bei hohen Überschallgeschwindigkeiten (Der Wirkungsgrad von Stossdiffusoren). Bericht Nr. 1005, Forschungen und Entwicklungen des Heereswaffenamtes, Kaiser Wilhelm-Inst. f. Stromungsforschung, Göttingen, Jan. 1944. (Pressure Recovery for Missles with Reaction Propulsion at High Supersonic Speeds (The Efficiency of Shock Diffusers). NACA TM 1140, 1947.

2. Kantrowitz, Arthur, and Donaldson, Coleman duP.: Preliminary Investigation of Supersonic Diffusers. NACA ACR L5D20, 1945.

3. Ferri, Antonio: Application of the Method of Characteristics to Supersonic Rotational Flow. NACA TN 1135, 1946.

4. Taylor, G. I., and Maccoll, J. W.: Velocity at Minimum Section. Vol. III of Aerodynamic Theory, div. H, ch. IV, sec. 4, W. F. Durand, ed., Julius Springer (Berlin), 1935, pp. 226-227. (Reprinted, C. I. T., Jan. 1943.)

5. Kantrowitz, Arthur: The Formation and Stability of Normal Shock Waves in Channel Flows. NACA TN 1225, 1947.

TABLE I - INLET DIMENSIONS AND SUMMARY

OF INLET-THROAT COMBINATIONS

NACA

Inlet-throat combination (1)	Inlet nose diameter a(fig. 1) (in.)	Inlet length b(fig. 1) (in.)	Throat length L(fig. 1) (in.)
5-1.190-0	1.682	1.605	0
10-1.190-0	1.682	.803	0
15-1.190-0	1.682	.531	0
20-1.190-0	1.682	.397	0
20-1.190-2	1.682	.397	2
30-1.190-0	1.682	.261	0
40-1.190-0	1.682	.192	0
5-1.176-0	1.672	1.489	0
5-1.176-1	1.672	1.489	1
5-1.176-2	1.672	1.489	2
5-1.176-4	1.672	1.489	4
10-1.176-0	1.672	.743	0
10-1.176-2	1.672	.743	2
15-1.176-0	1.672	.494	0
15-1.176-2	1.672	.494	2
20-1.176-0	1.672	.369	0
20-1.176-2	1.672	.369	2
Cylindrical	1.542	.855	0
Diverging	1.453	1.021	0

[1]The first numeral indicates the included convergence angle of the inlet τ, the second numeral gives the geometrical contraction ratio of the inlet (nose area/minimum area), and the third numeral shows the length of straight throat section L.

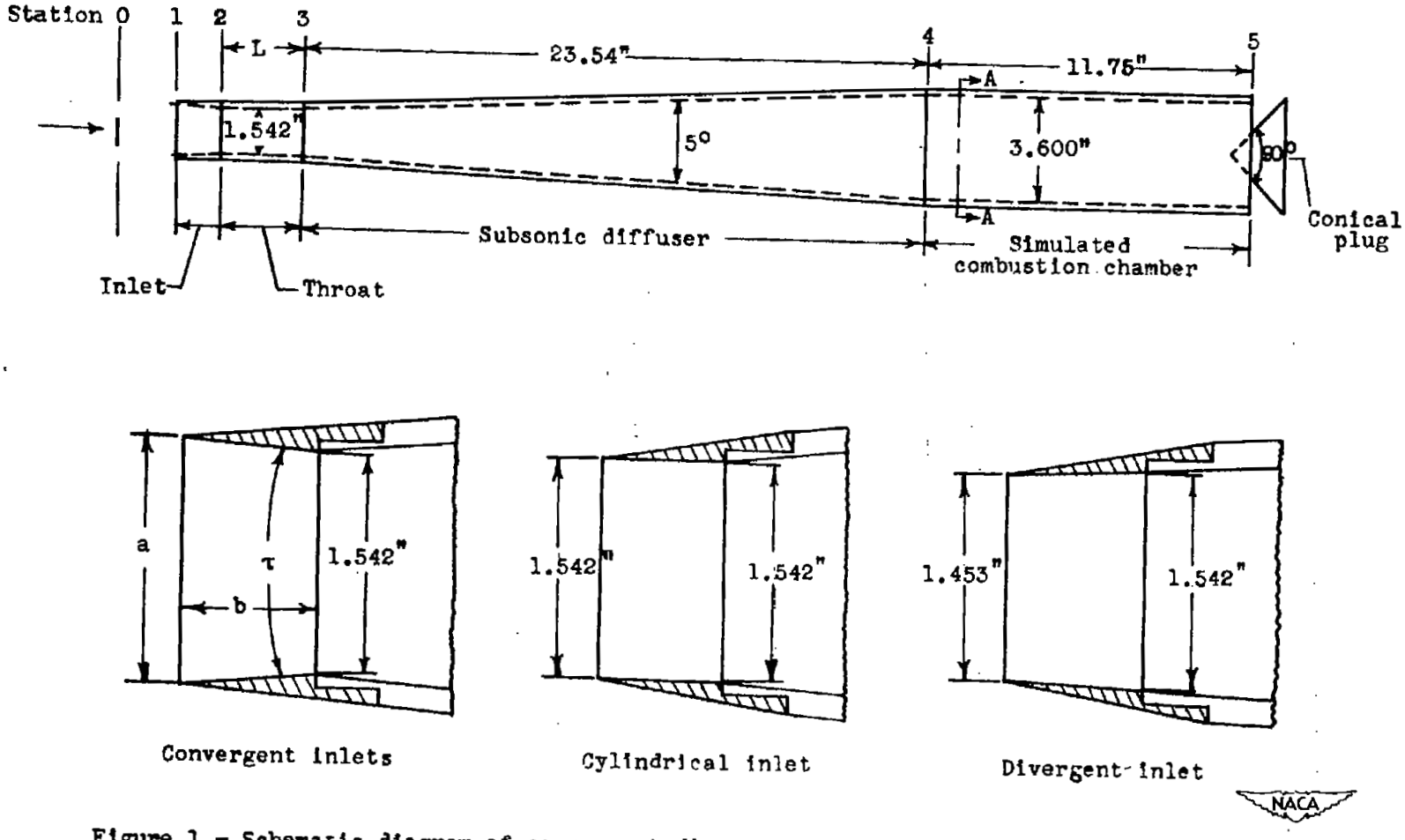

Figure 1.- Schematic diagram of convergent-divergent diffuser model and sketch of inlets tested. (See table I for values of a, b, L, and τ.)

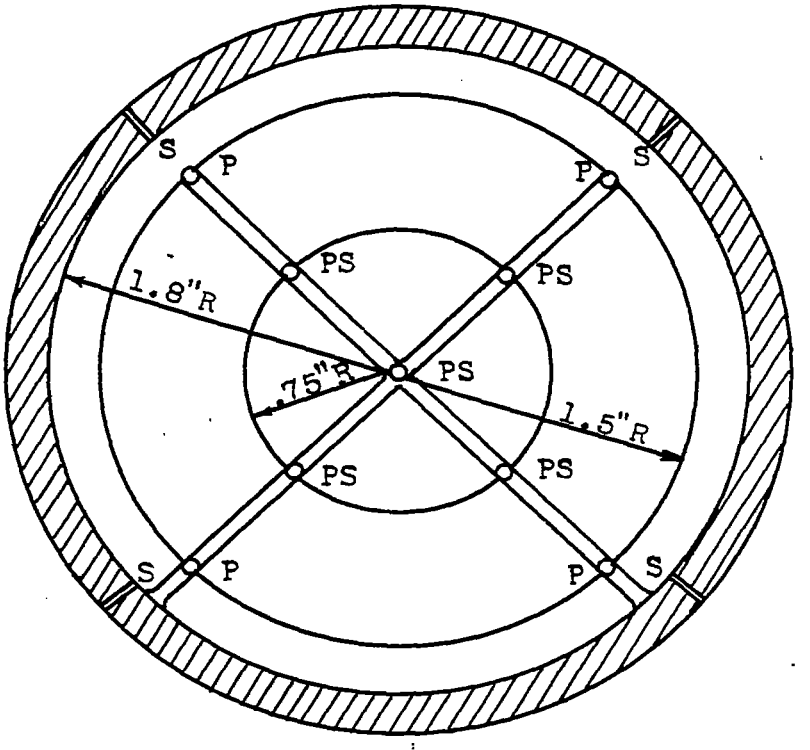

Section A-A
(See fig. 1.)

P Pitot tube
S Static-pressure orifice
PS Pitot-static tube

Figure 2.- Instrumentation at combustion-chamber inlet.

(a) A_5/A_1, 0.650.

(b) A_5/A_1, 0.850.

NACA
C-14410
3-8-46

(c) A_5/A_1, 1.090.

Figure 3. - Schlieren photographs of air flow about diffuser inlet for several outlet-inlet area ratios, A_5/A_1. M_0, 1.85; angle of attack, 5°.

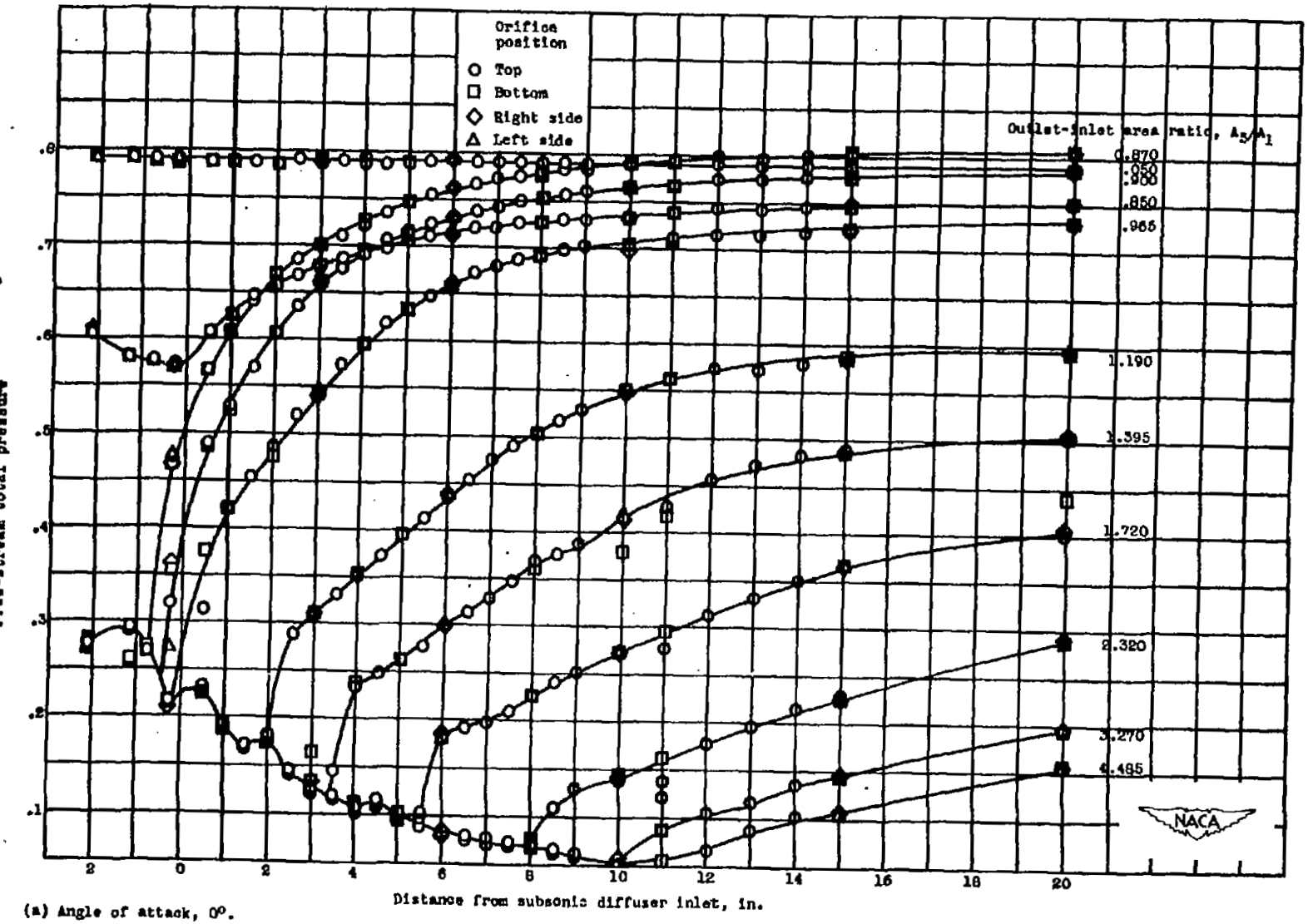

(a) Angle of attack, 0°.

Figure 4.- Static-pressure distribution along diffuser for several outlet areas with 20-1.190-2 configuration.

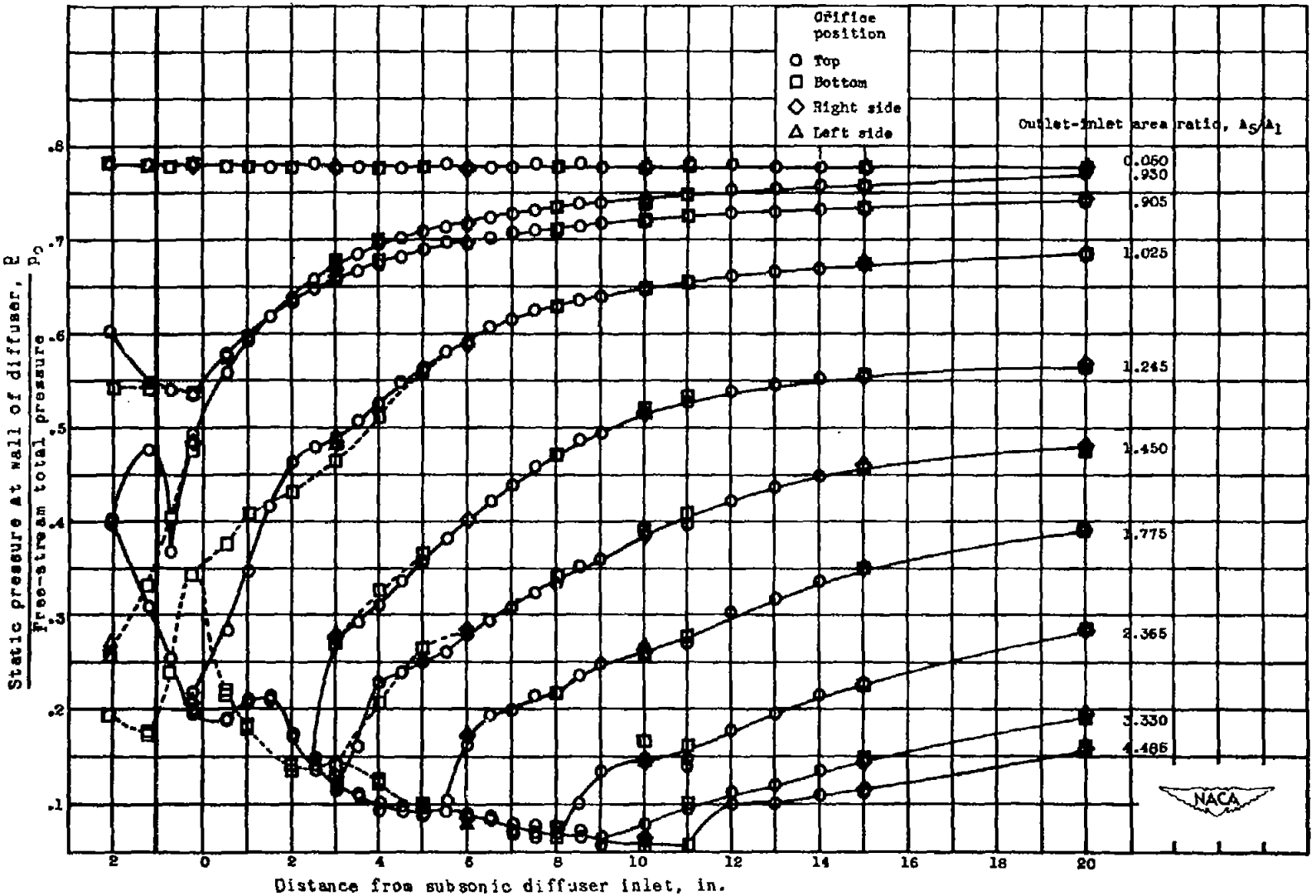

(b) Angle of attack, 5°.

Figure 4. - Concluded. Static-pressure distribution along diffuser for several outlet areas with 20-1.190-2 configuration.

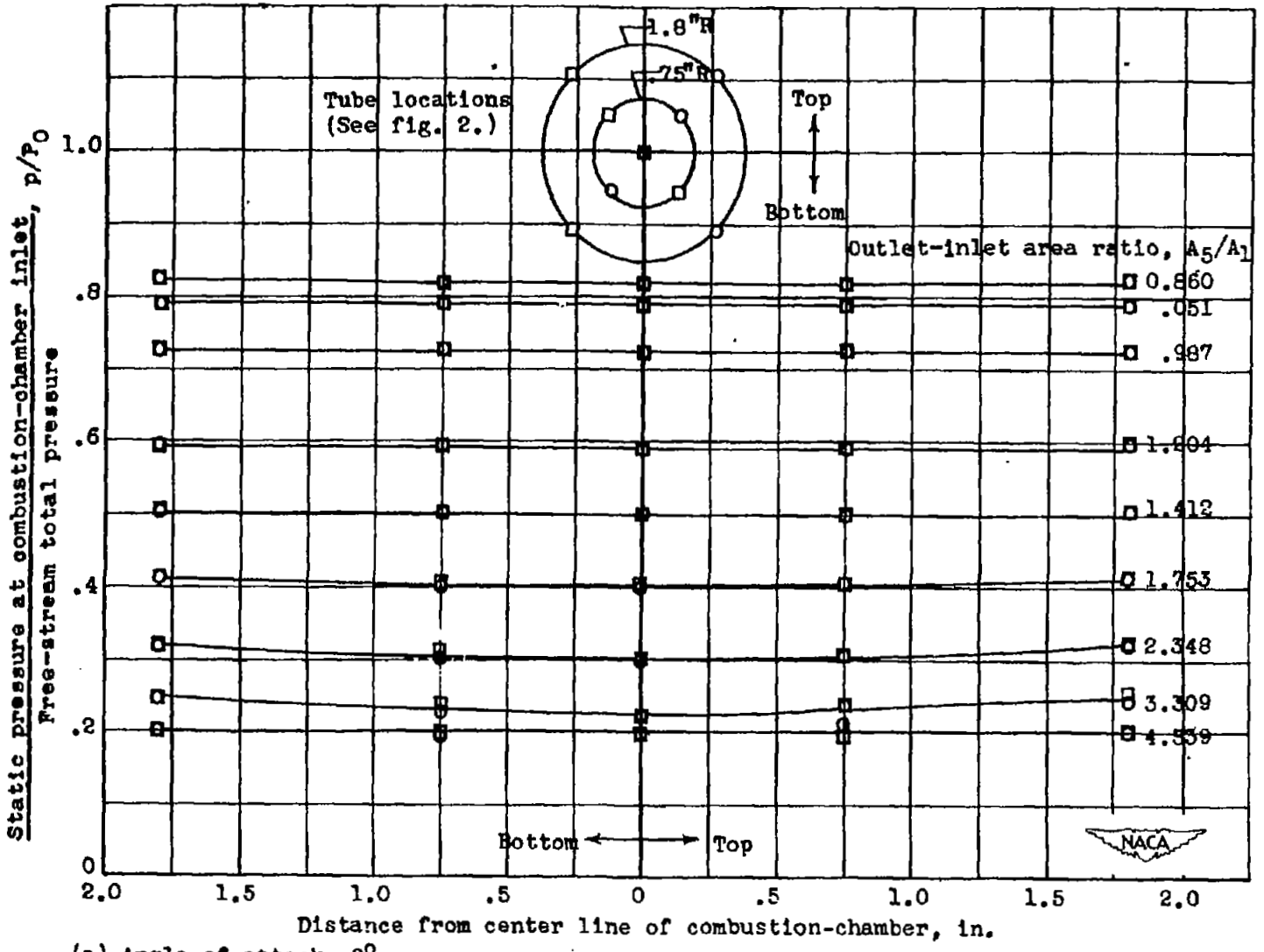

(a) Angle of attack, 0°.

Figure 5.- Static-pressure distribution at combustion-chamber inlet for several outlet areas with 5-1.176-2 configuration.

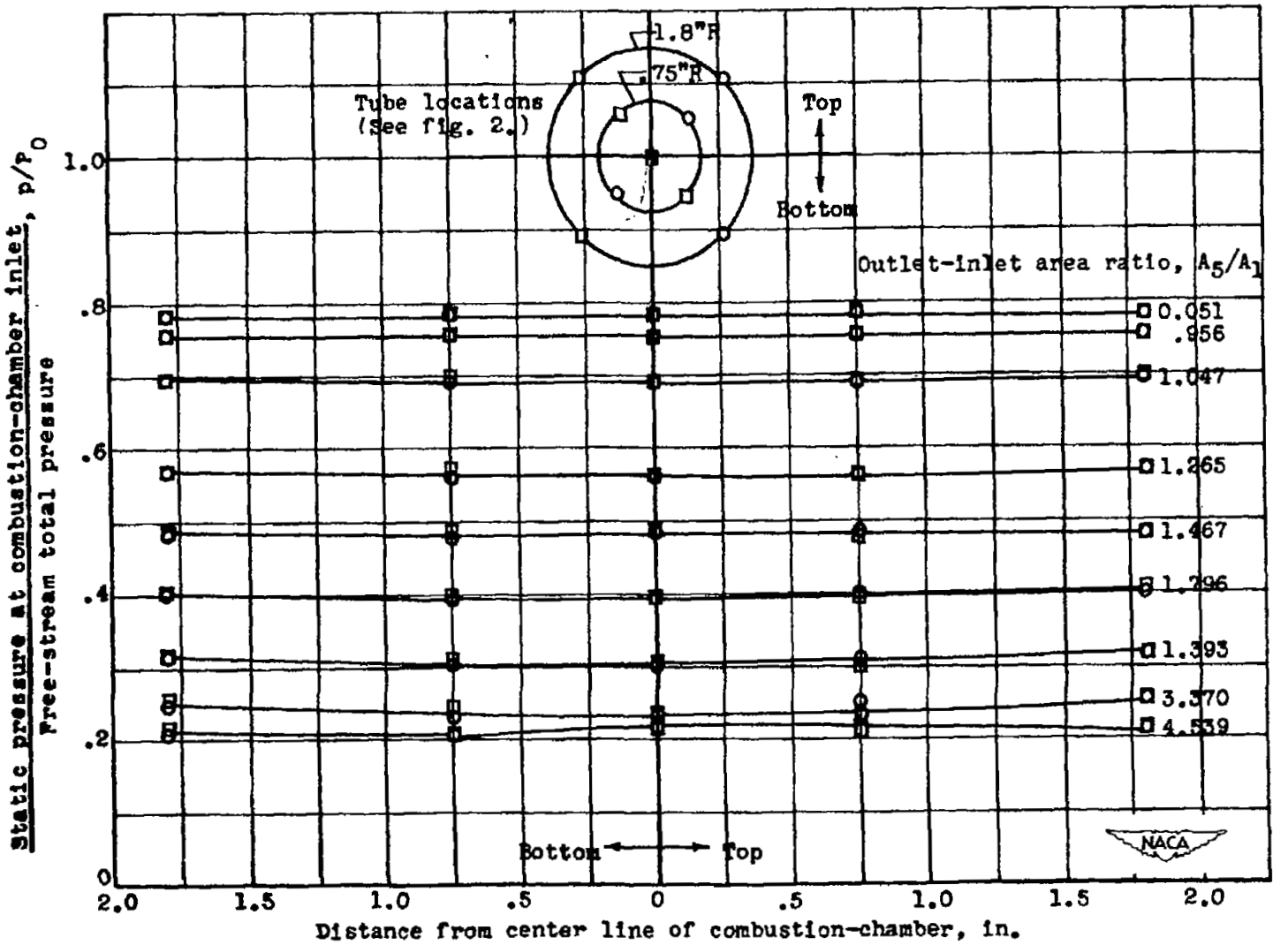

(b) Angle of attack, 5°.

Figure 5.- Concluded. Static-pressure distribution at combustion-chamber inlet for several outlet areas with 5-1.176-2 configuration.

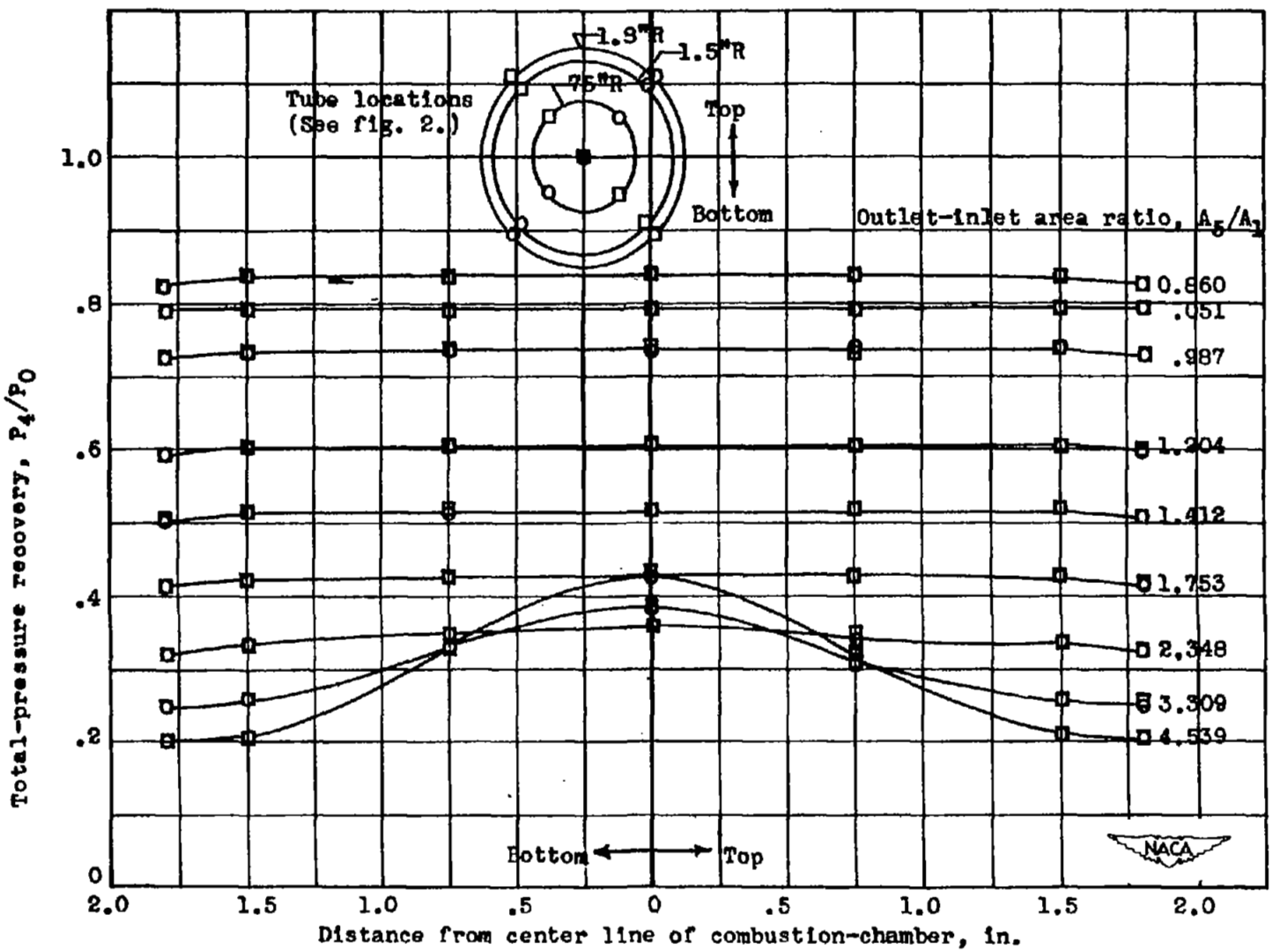

(a) Angle of attack, 0°.

Figure 6.- Total-pressure distribution at combustion-chamber inlet for several outlet areas with 5-1.176-2 configuration.

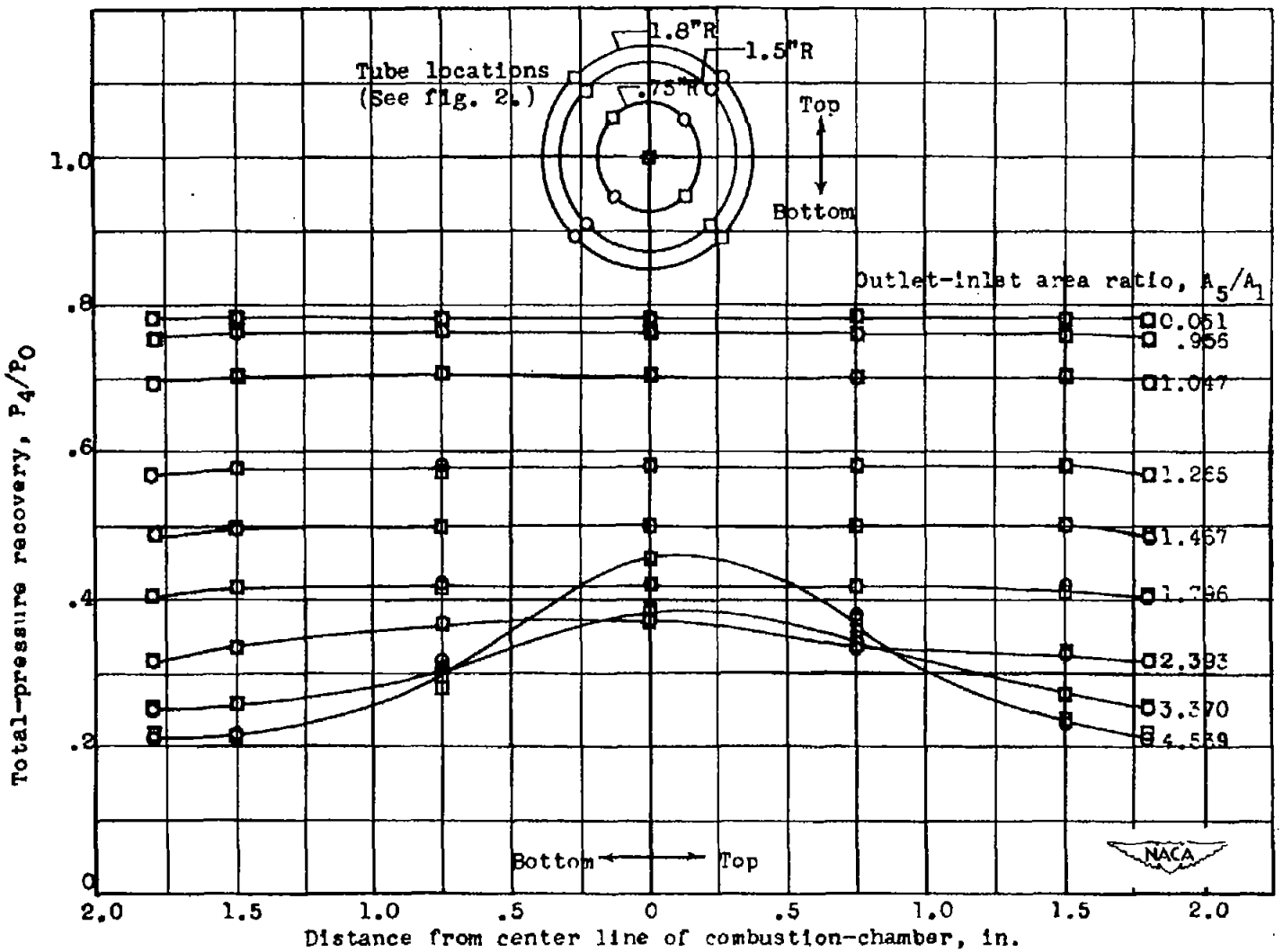

(b) Angle of attack, 5°.

Figure 6.- Concluded. Total-pressure distribution at combustion-chamber inlet for several outlet areas with 5-1.176-2 configuration.

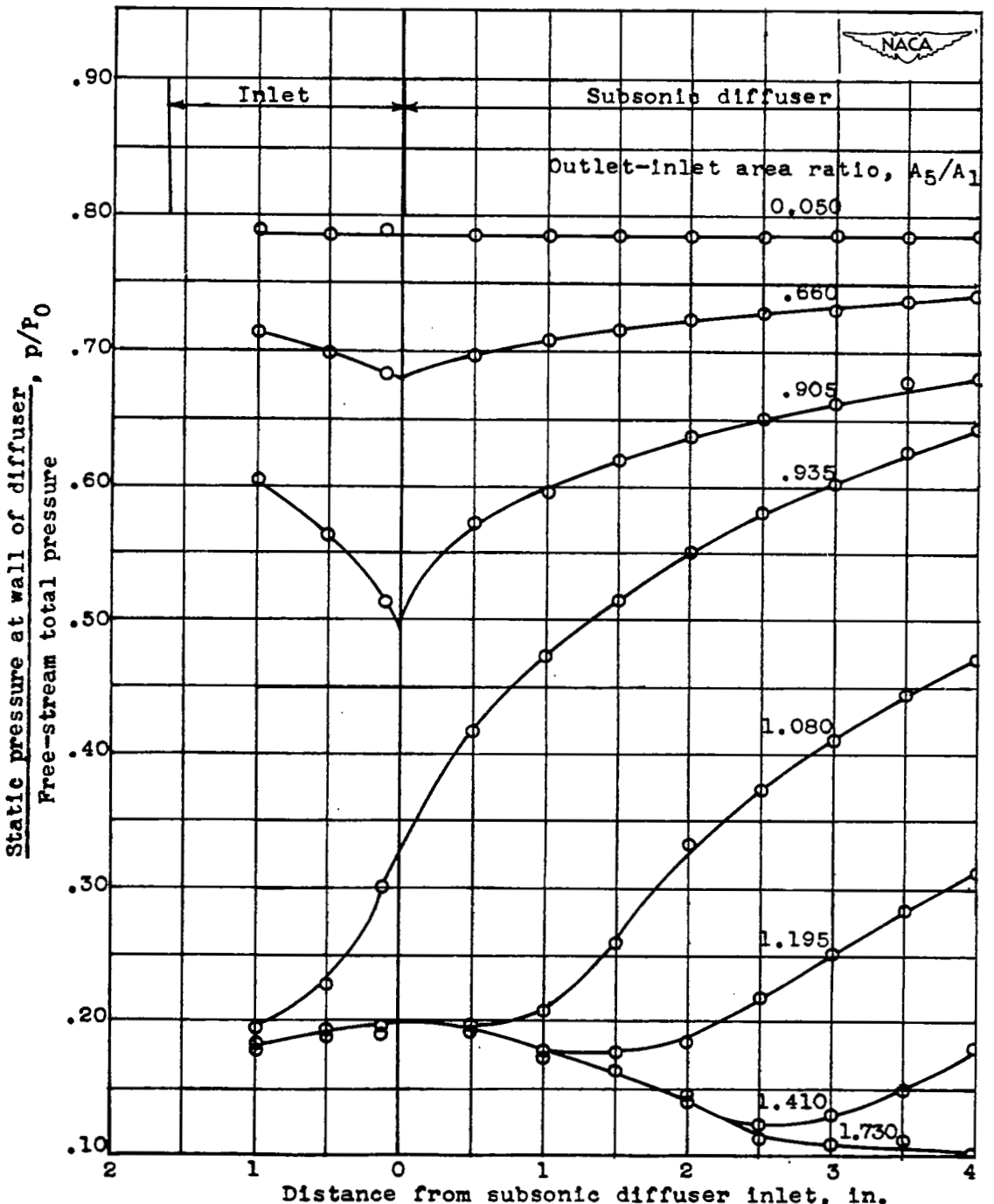

(a) 5-1.190-0 configuration.

Figure 7.- Static-pressure distribution along top of inlet and subsonic diffuser with no throat at angle of attack of 0°.

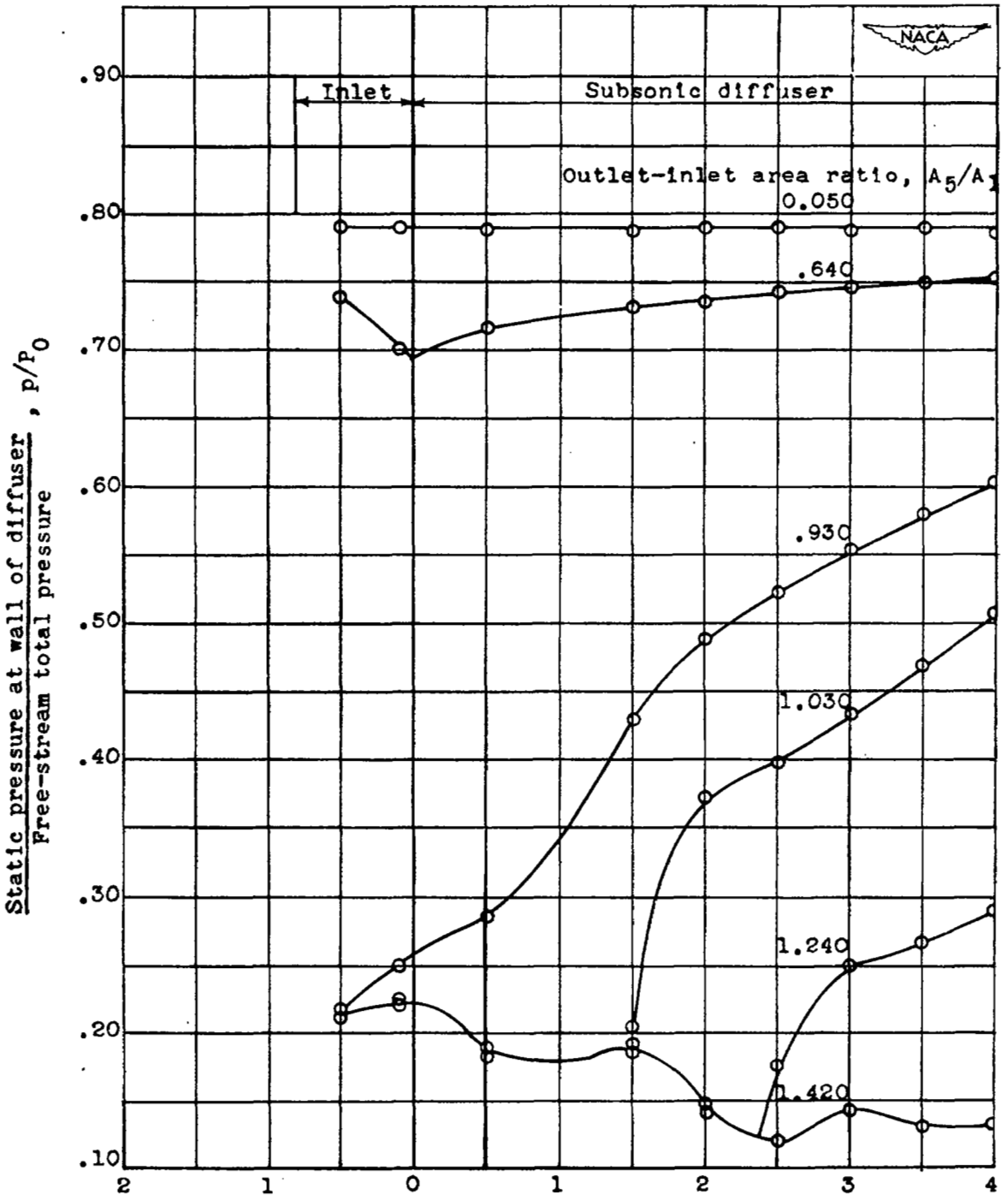

(b) 10-1.190-0 configuration.

Figure 7.- Continued. Static-pressure distribution along top of inlet and subsonic diffuser with no throat at angle of attack of 0°.

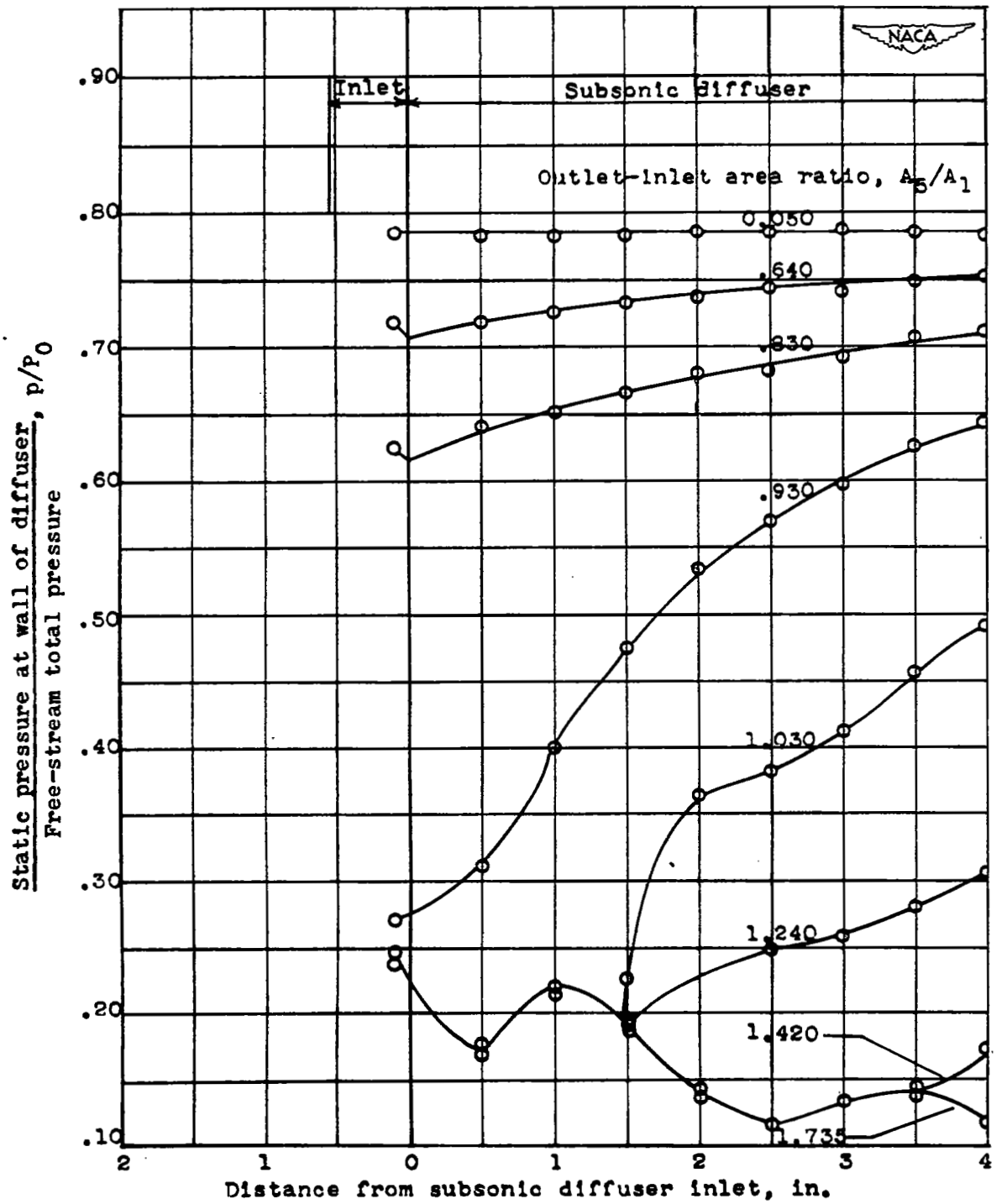

(c) 15-1.190-0 configuration.

Figure 7.- Continued. Static-pressure distribution along top of inlet and subsonic diffuser with no throat at angle of attack of 0°.

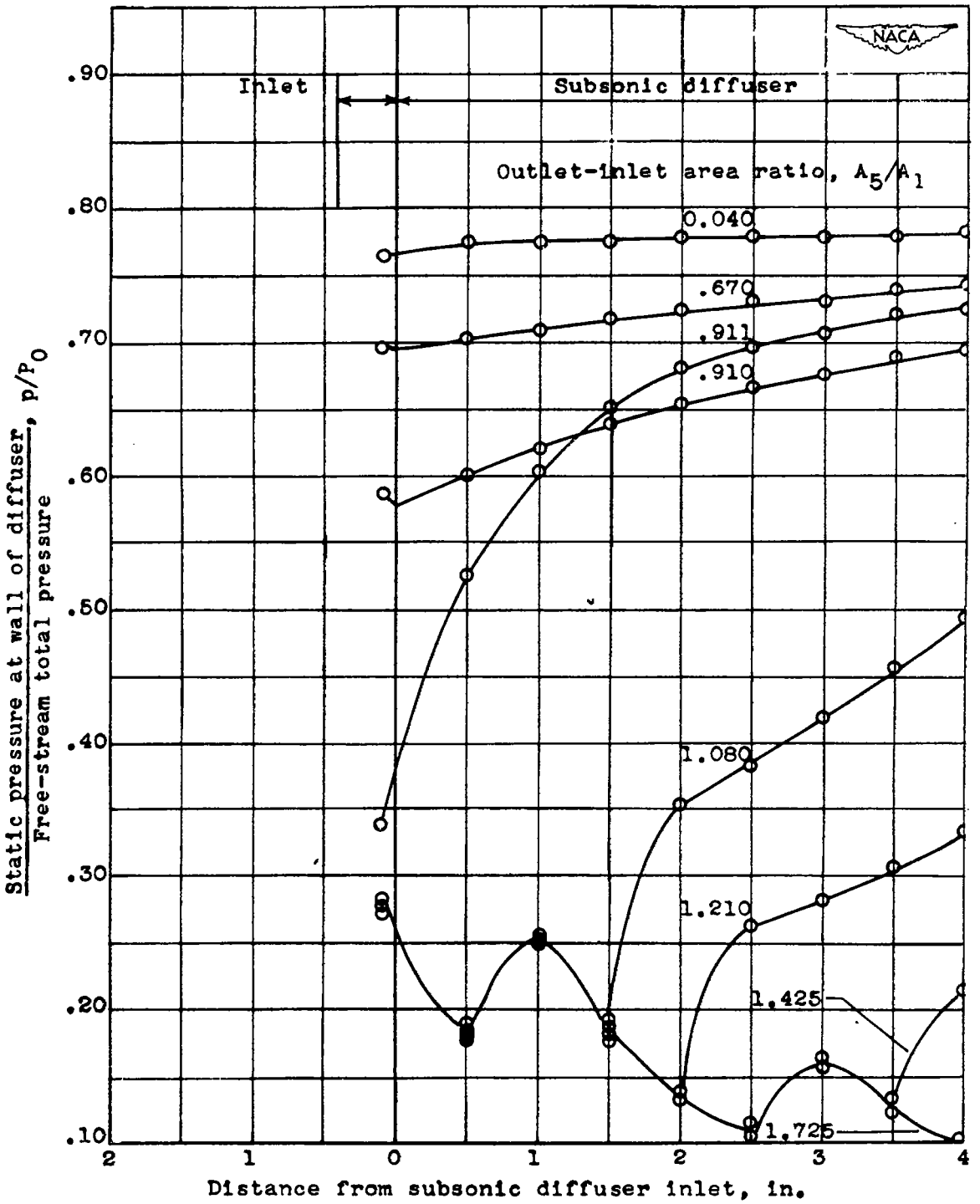

(d) 20-1.190-0 configuration.

Figure 7.- Continued. Static-pressure distribution along top of inlet and subsonic diffuser with no throat at angle of attack of 0°.

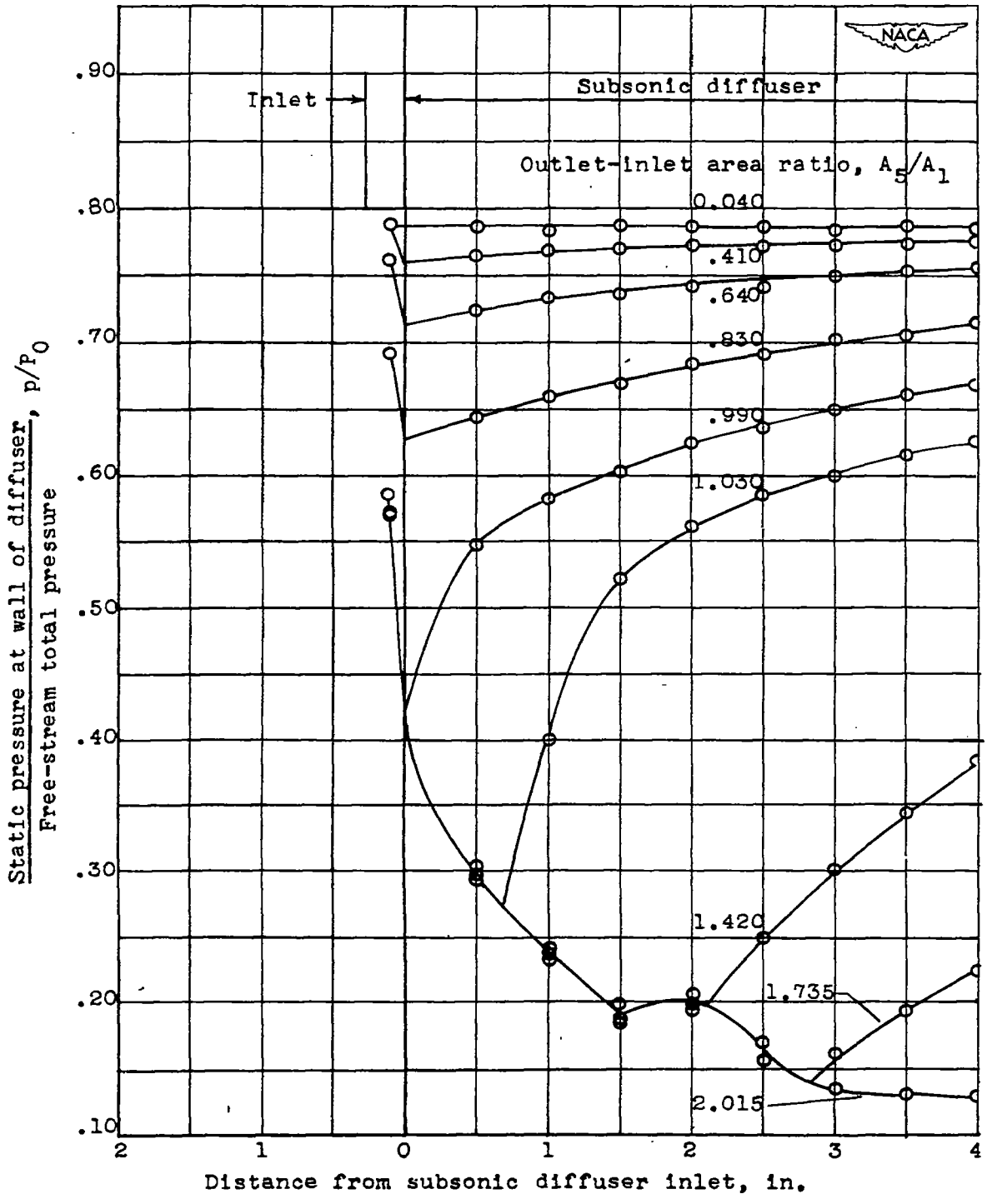

(e) 30-1.190-0 configuration.

Figure 7.- Continued. Static-pressure distribution along top of inlet and subsonic diffuser with no throat at angle of attack of 0°.

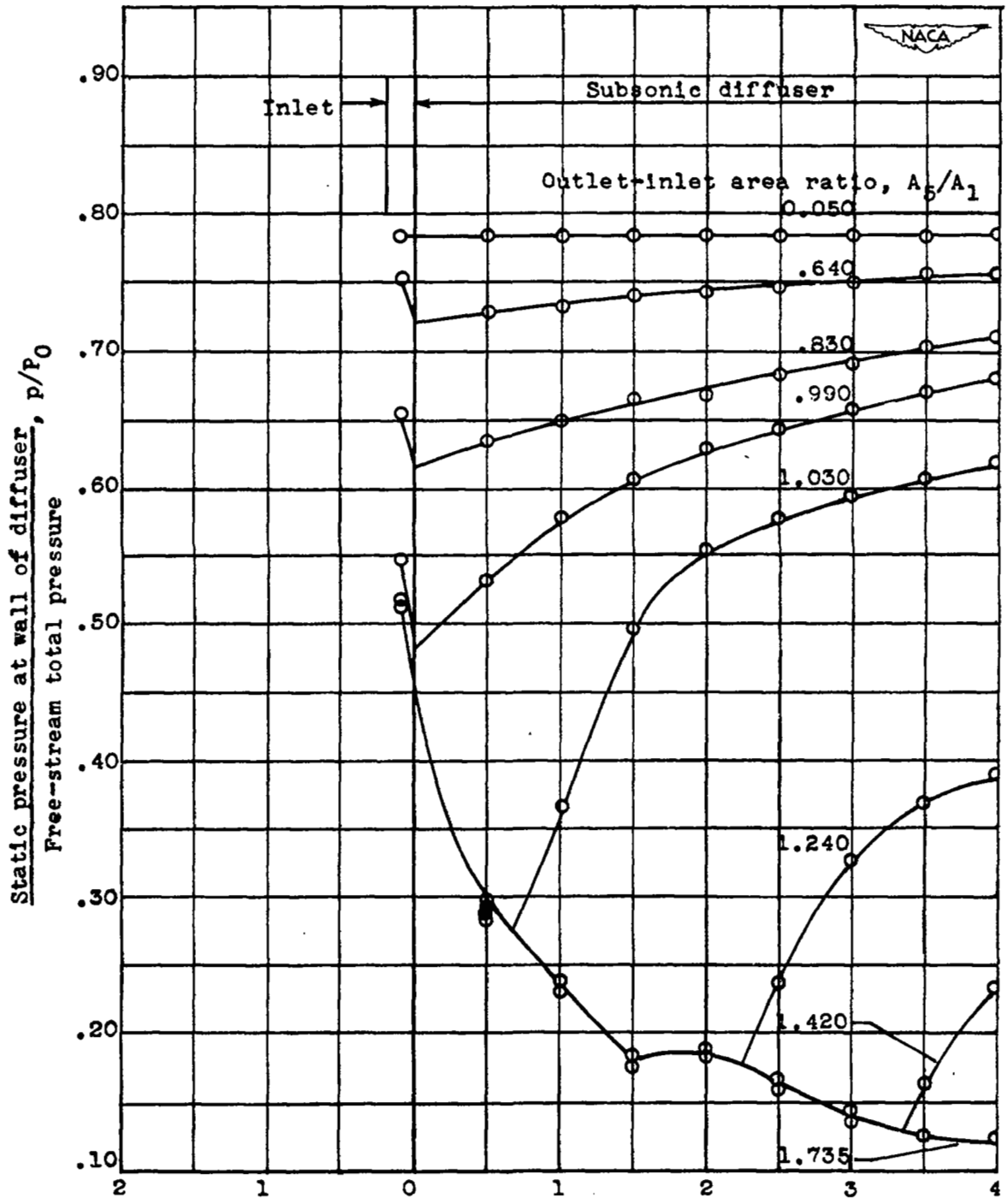

(f) 40-1.190-0 configuration.

Figure 7.- Concluded. Static-pressure distribution along top of inlet and subsonic diffuser with no throat at angle of attack of 0°.

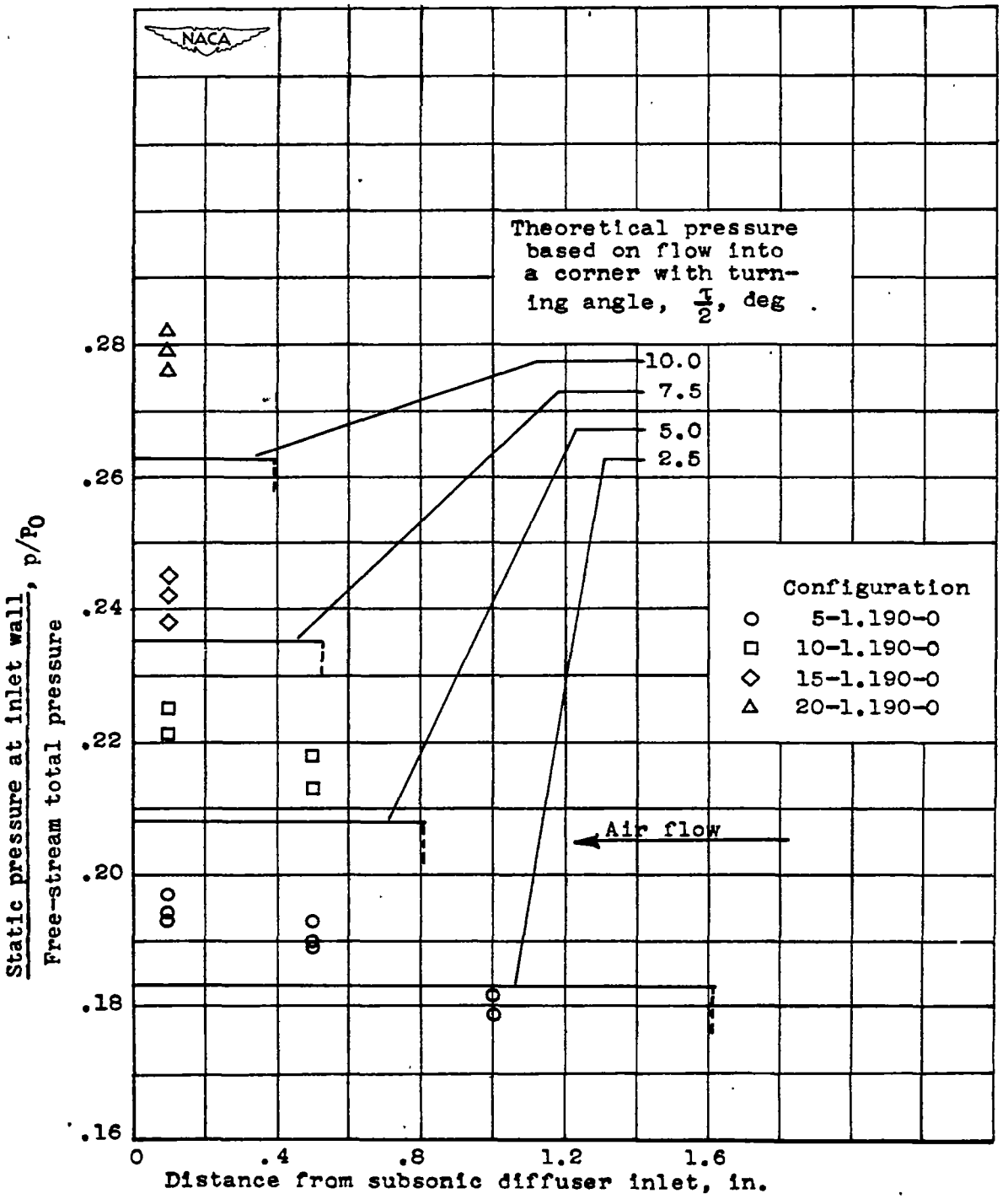

Figure 8.- Comparison of theoretical and measured static pressures in diffuser inlets with no throat at angle of attack of 0°.

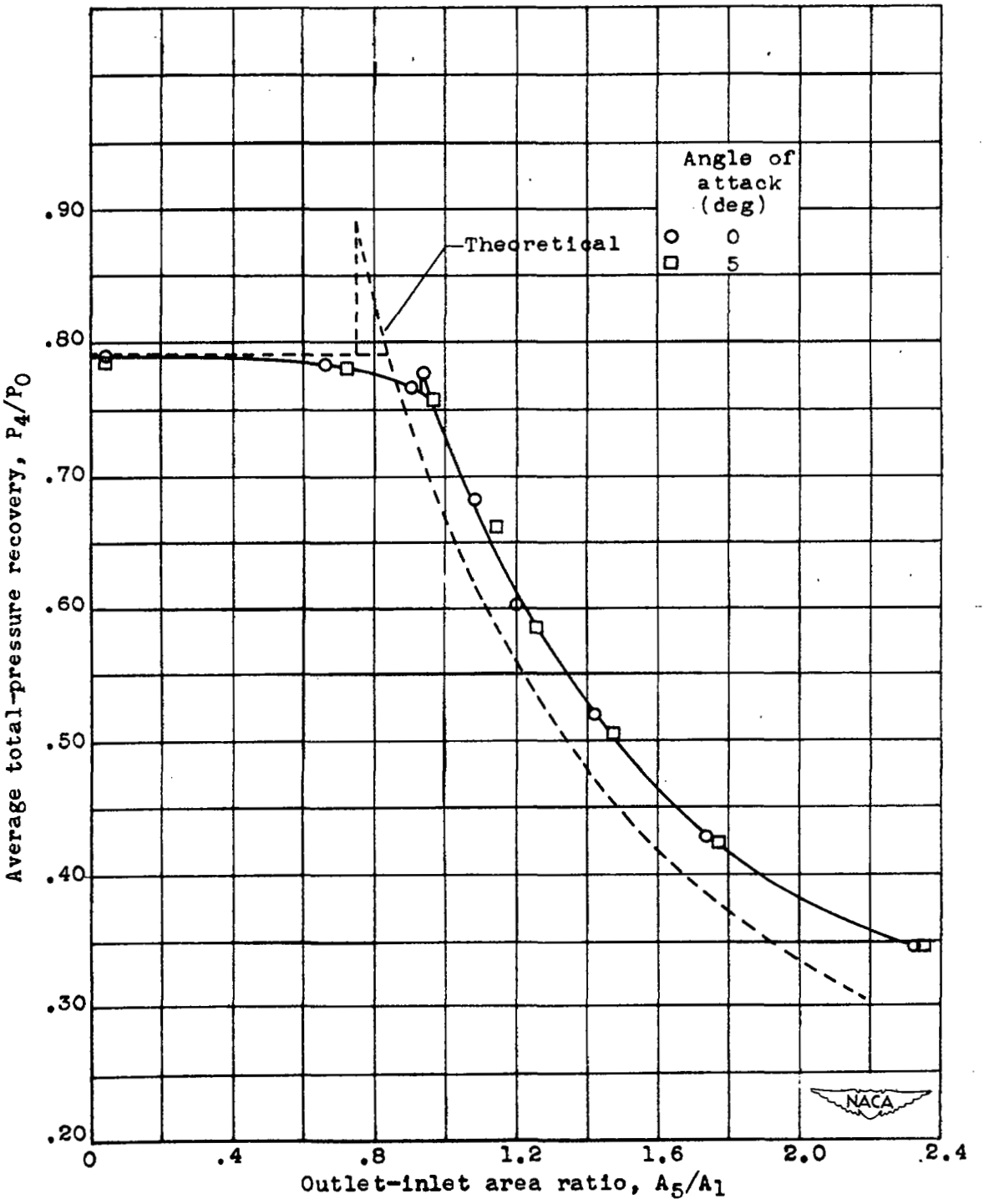

(a) 5-1.190-0 configuration.

Figure 9.- Effect of combustion-chamber-outlet area on average total-pressure recovery with no throat at contraction ratio of 1.190.

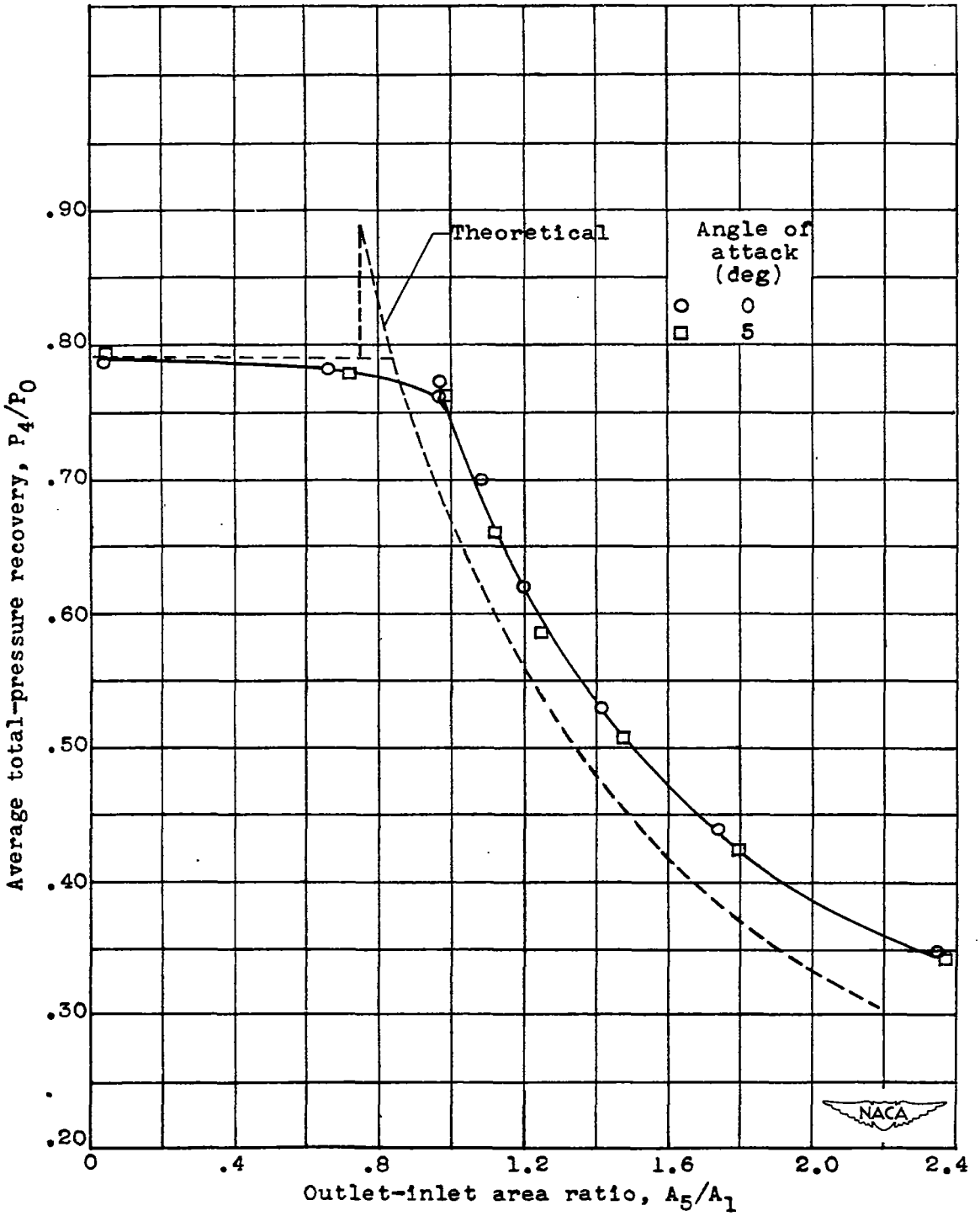

(b) 10-1.190-0 configuration.

Figure 9.- Continued. Effect of combustion-chamber-outlet area on average total-pressure recovery with no throat at contraction ratio of 1.190.

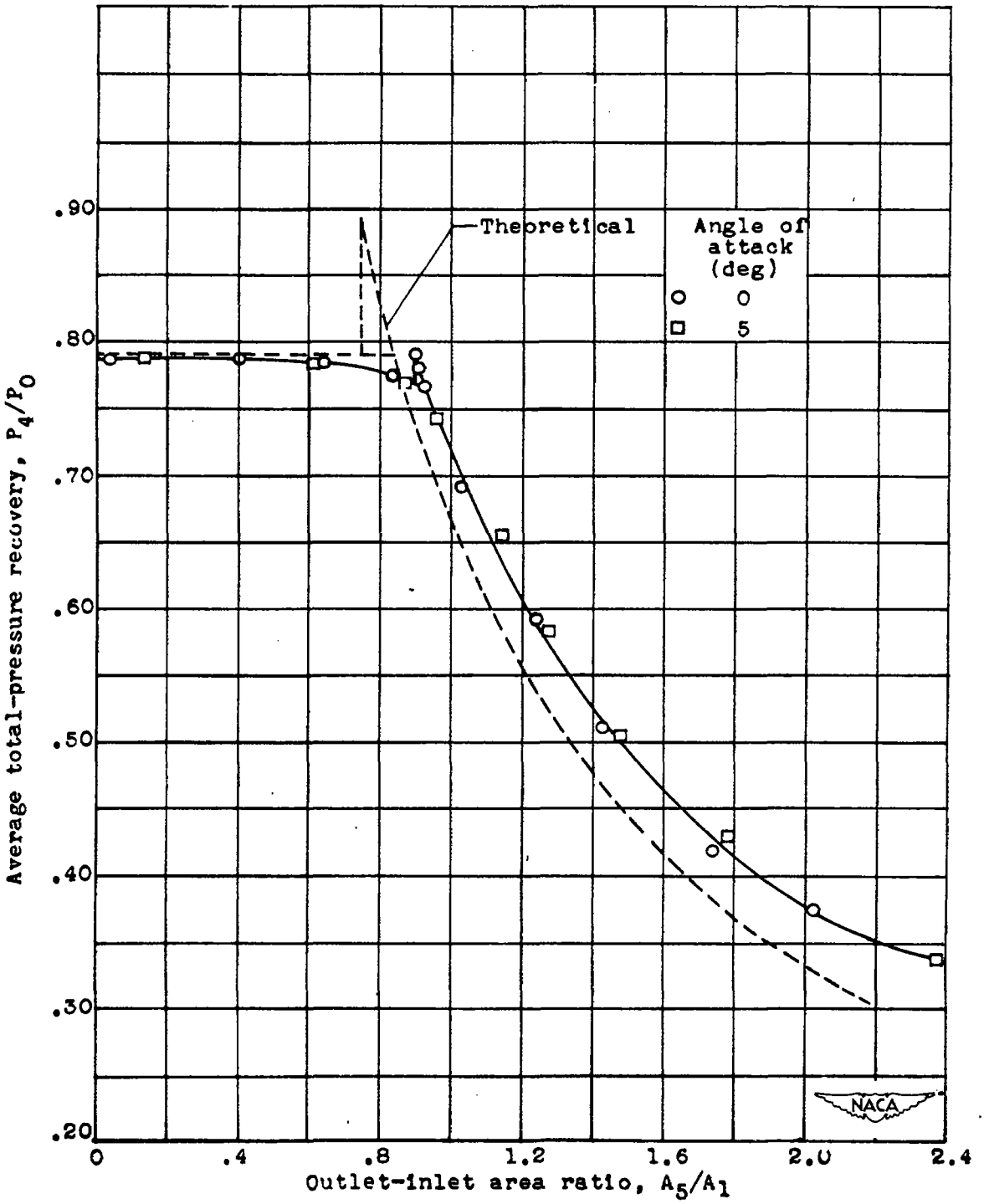

(c) 15-1.190-0 configuration.

Figure 9.- Continued. Effect of combustion-chamber-outlet area on average total-pressure recovery with no throat at contraction ratio of 1.190.

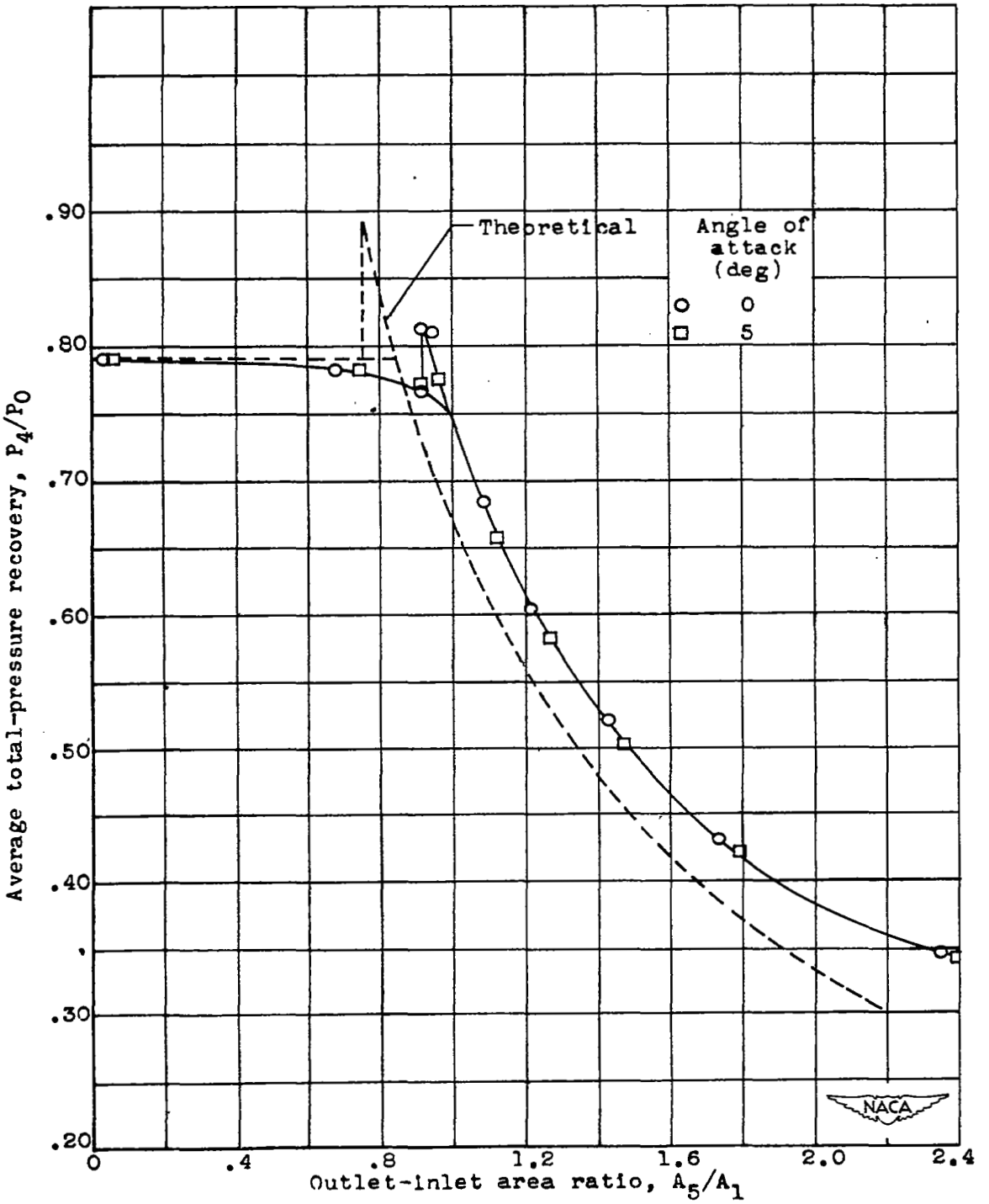

(d) 20-1.190-0 configuration.

Figure 9.- Continued. Effect of combustion-chamber-outlet area on average total-pressure recovery with no throat at contraction ratio of 1.190.

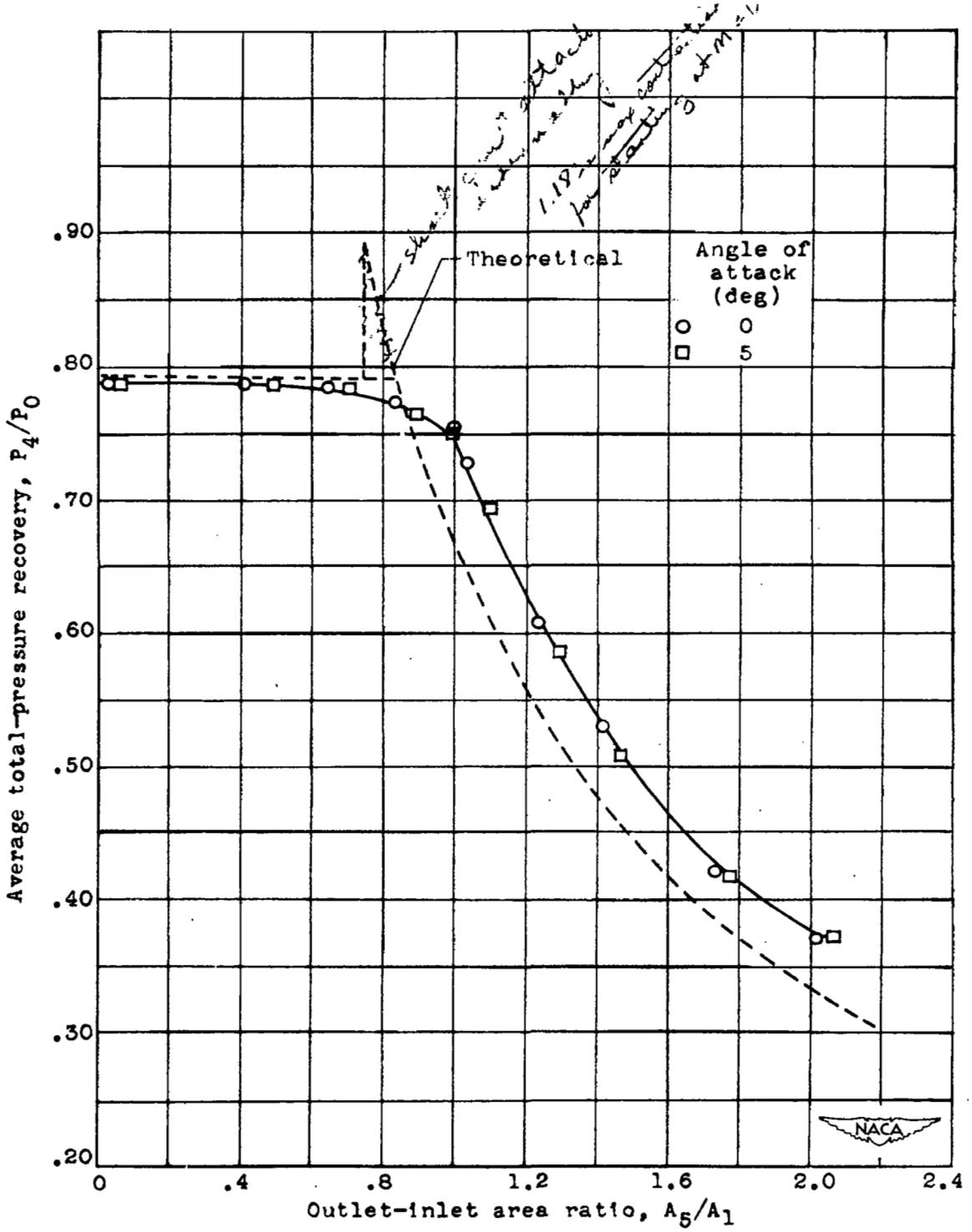

(e) 30-1.190-0 configuration.

Figure 9.- Continued. Effect of combustion-chamber-outlet area on average total-pressure recovery with no throat at contraction ratio of 1.190.

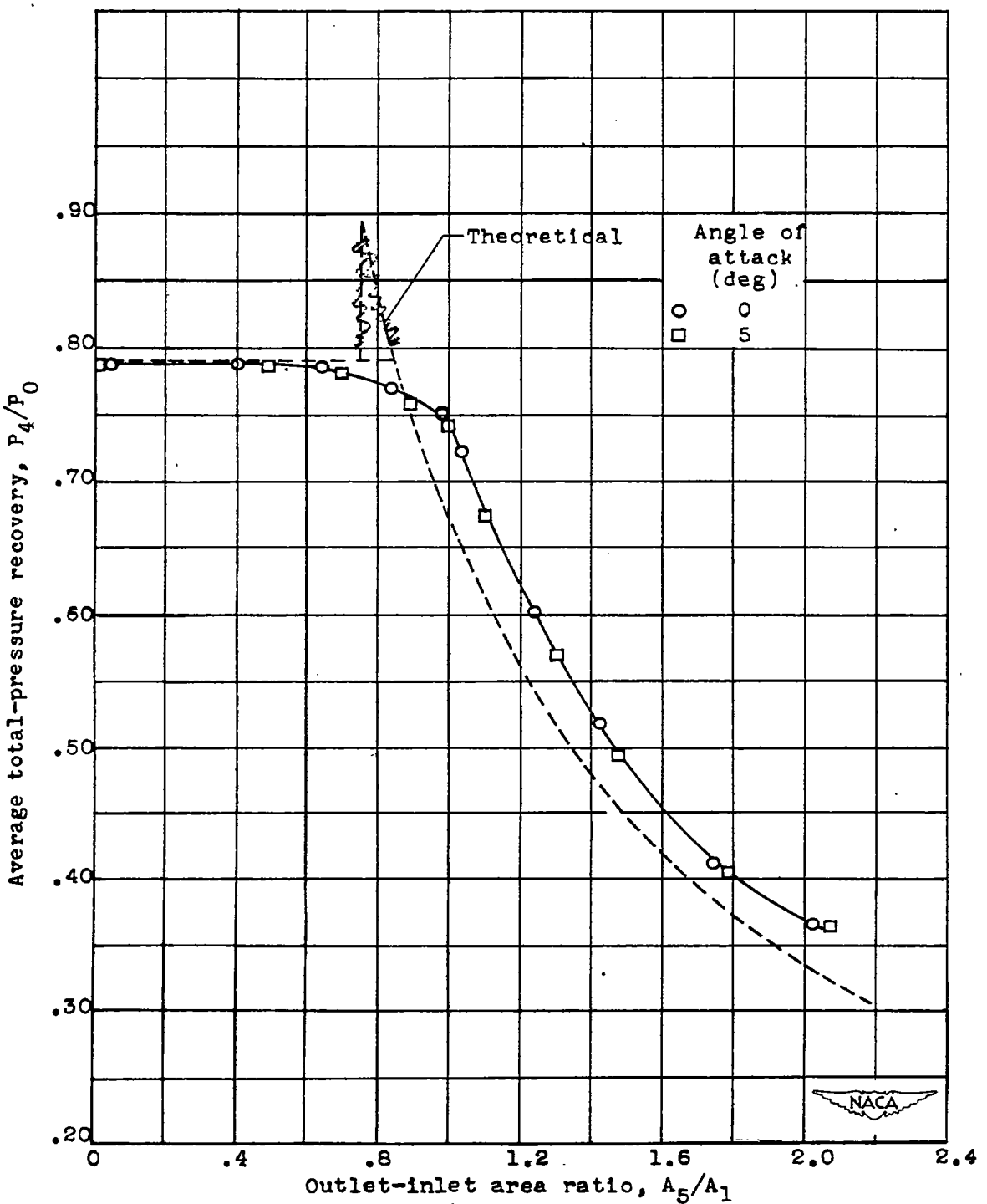

(f) 40-1.190-0 configuration.

Figure 9.- Concluded. Effect of combustion-chamber-outlet area on average total-pressure recovery with no throat at contraction ratio of 1.190.

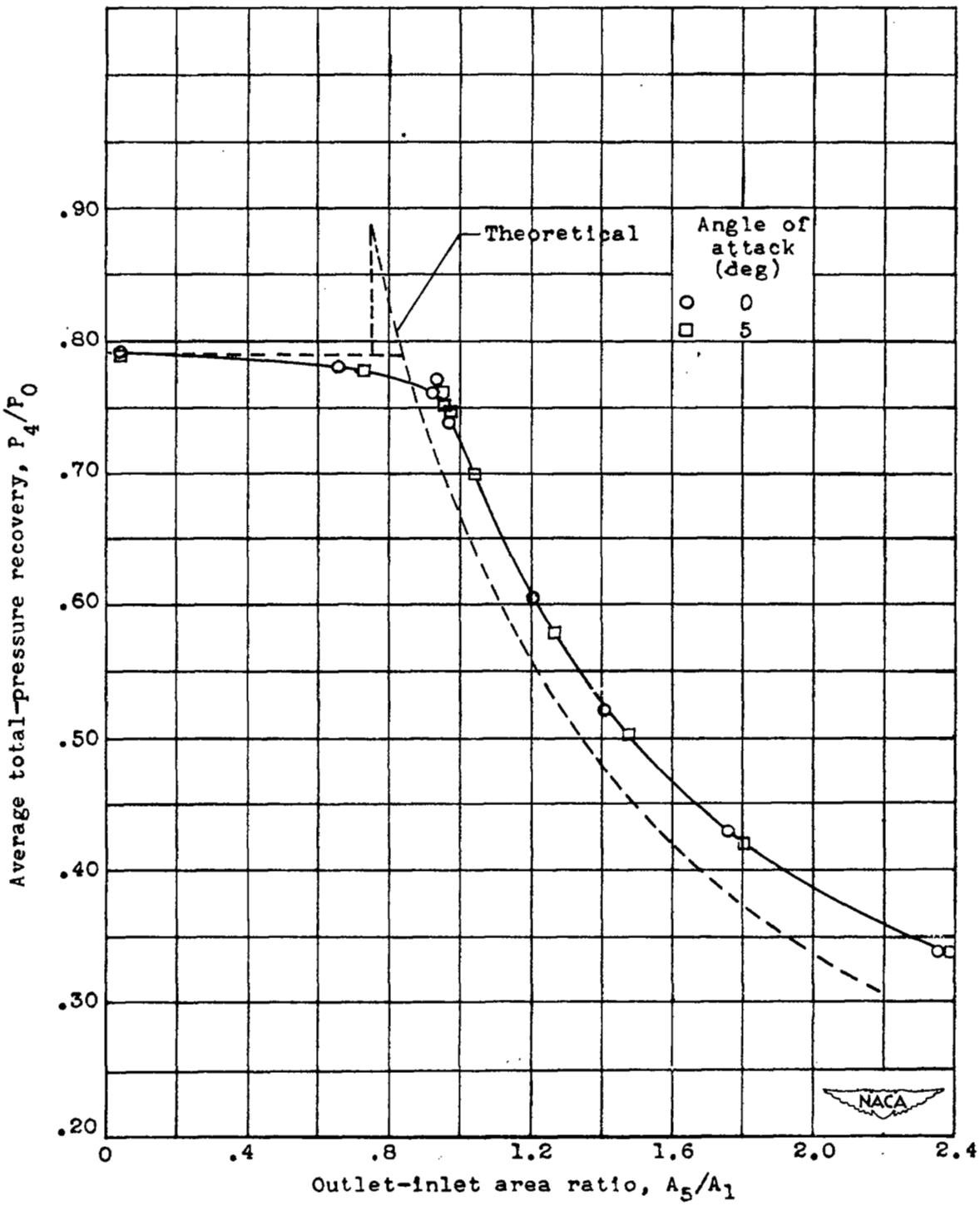

(a) 5-1.176-0 configuration.

Figure 10.- Effect of combustion-chamber-outlet area on average total-pressure recovery with no throat at contraction ratio of 1.176.

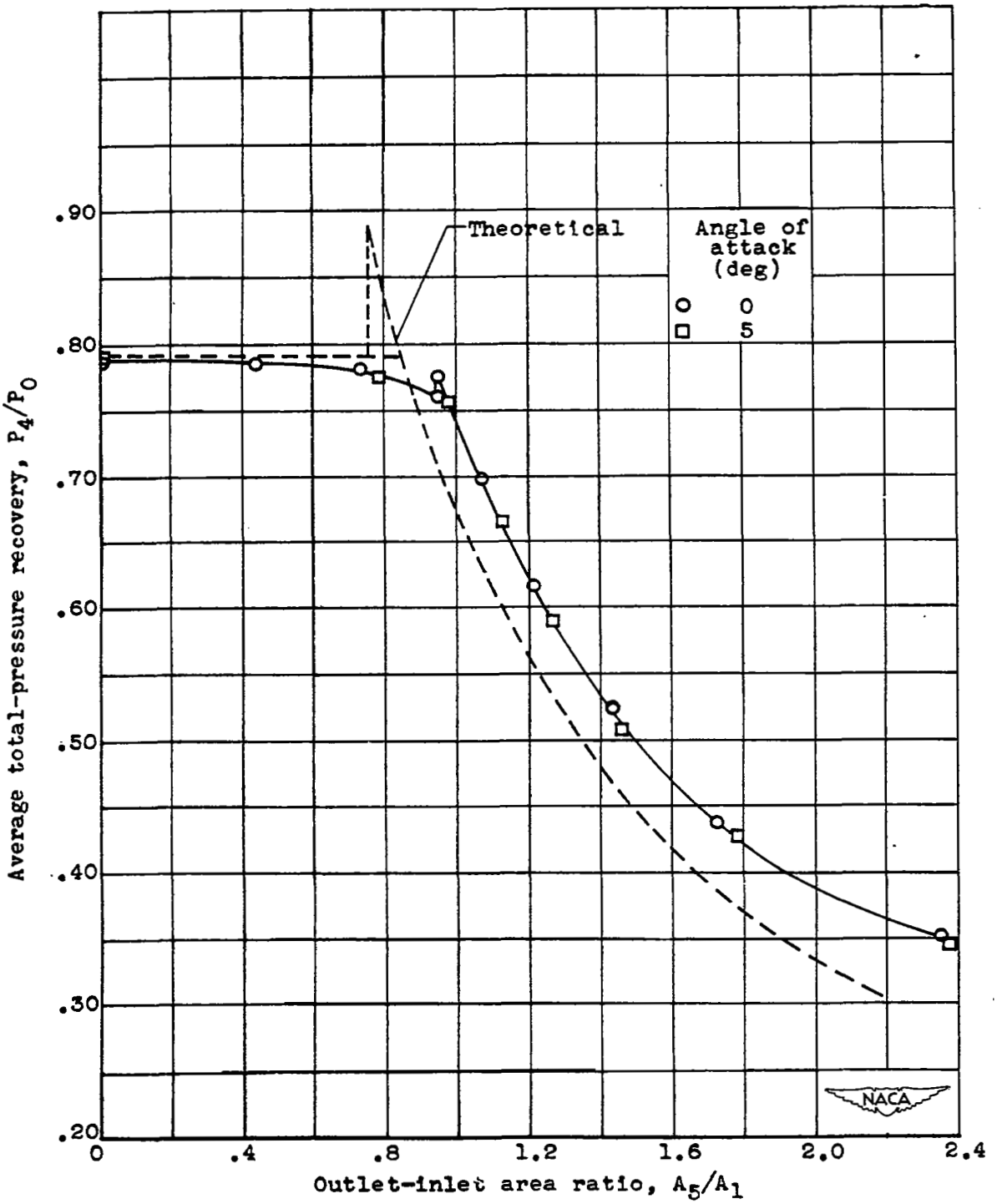

(b) 10-1.176-0 configuration.

Figure 10.- Continued. Effect of combustion-chamber-outlet area on average total-pressure recovery with no throat at contraction ratio of 1.176.

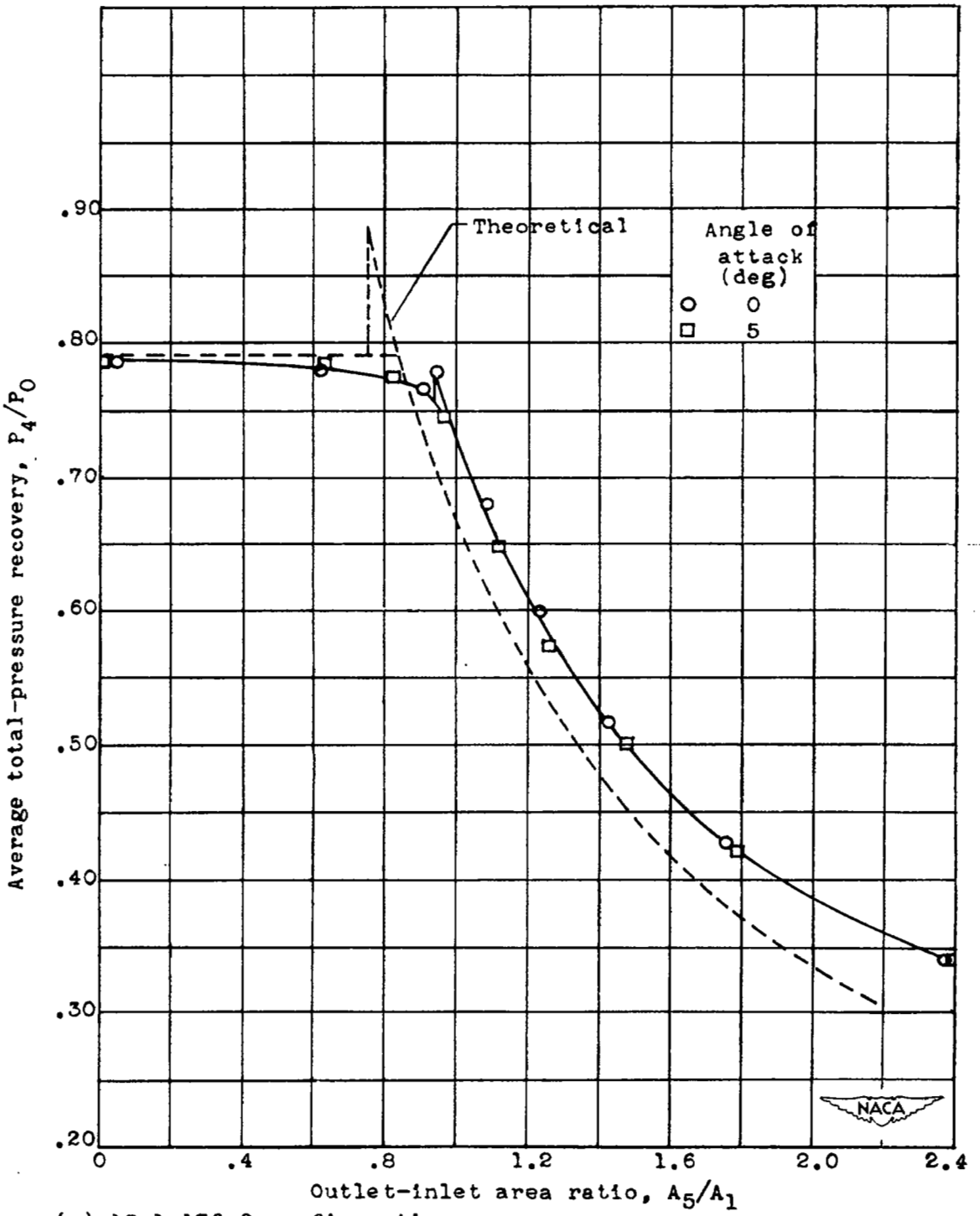

(c) 15-1.176-0 configuration.

Figure 10.- Continued. Effect of combustion-chamber-outlet area on average total-pressure recovery with no throat at contraction ratio of 1.176.

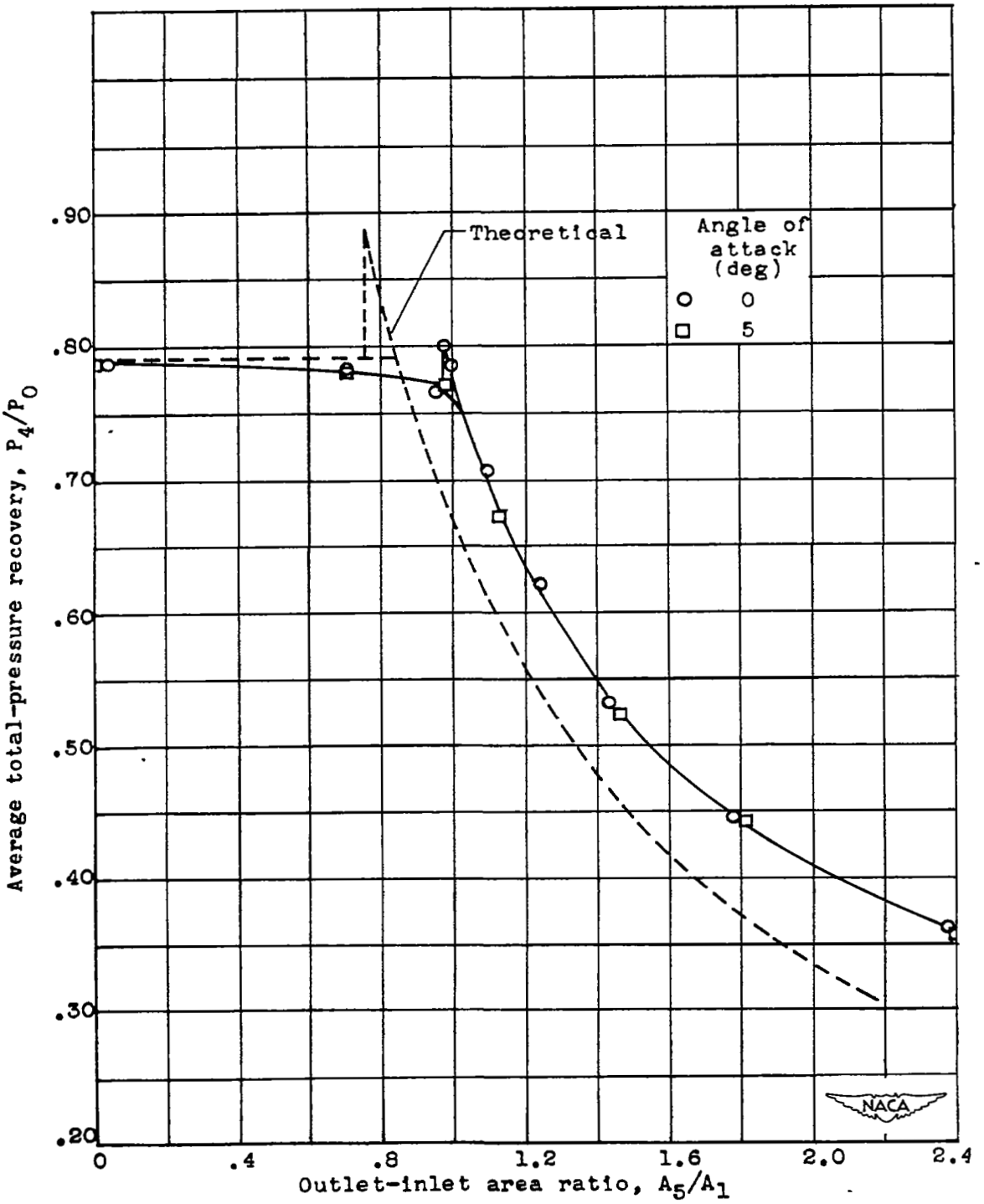

(d) 20-1.176-0 configuration.

Figure 10.- Concluded. Effect of combustion-chamber-outlet area on average total-pressure recovery with no throat at contraction ratio of 1.176.

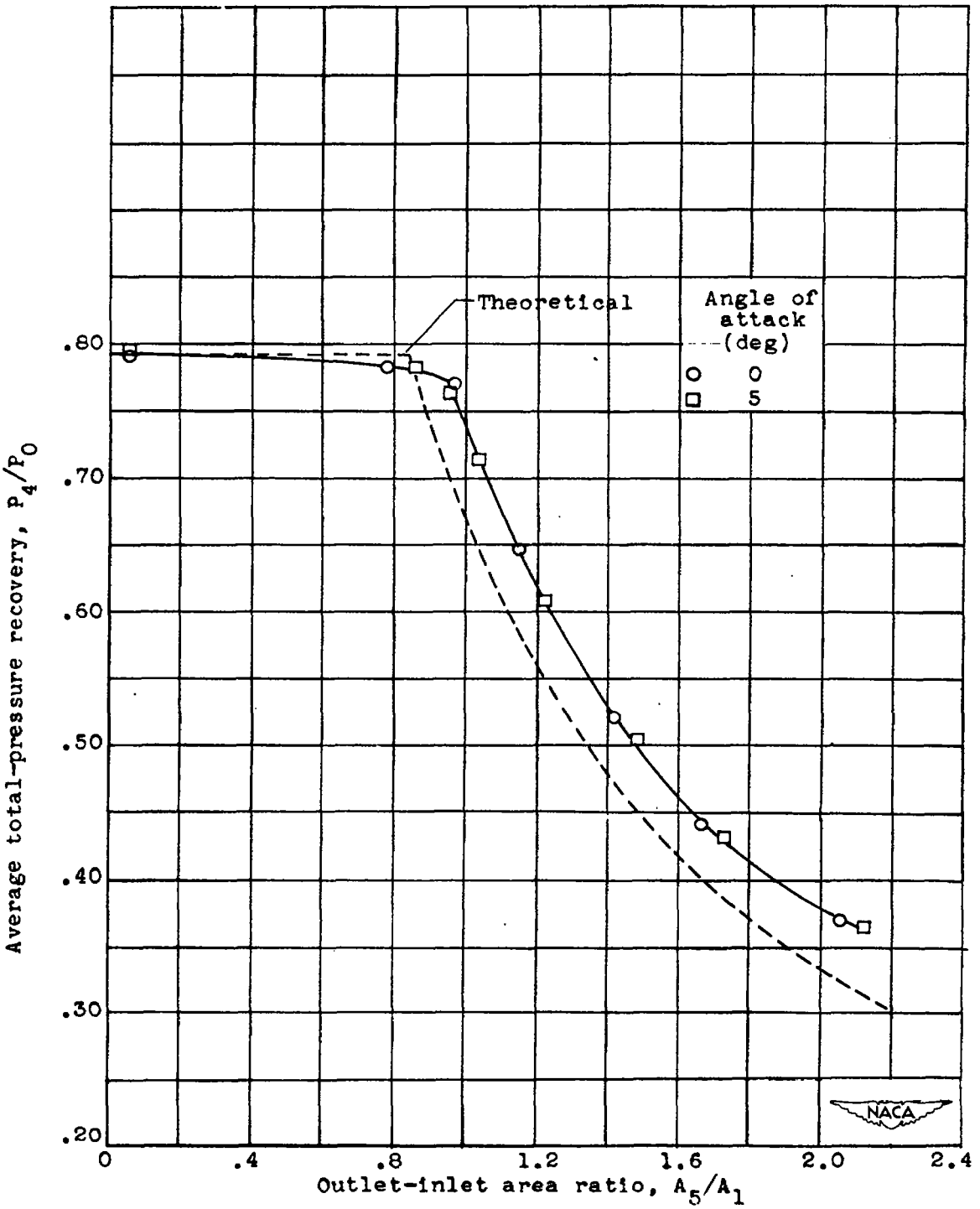

Figure 11.- Effect of combustion-chamber-outlet area on average total-pressure recovery with no throat and cylindrical inlet.

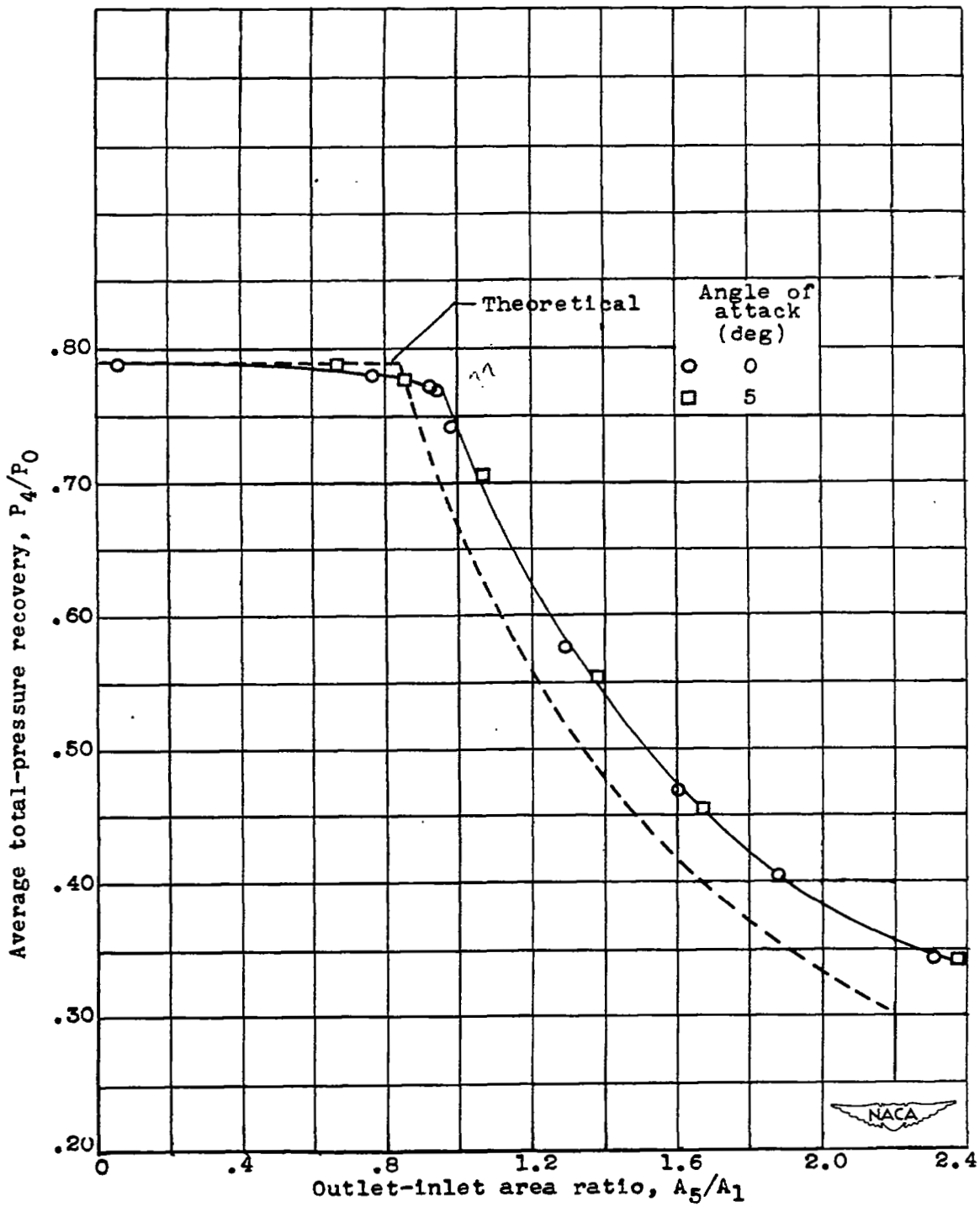

Figure 12.- Effect of combustion-chamber-outlet area on average total-pressure recovery with no throat and diverging inlet.

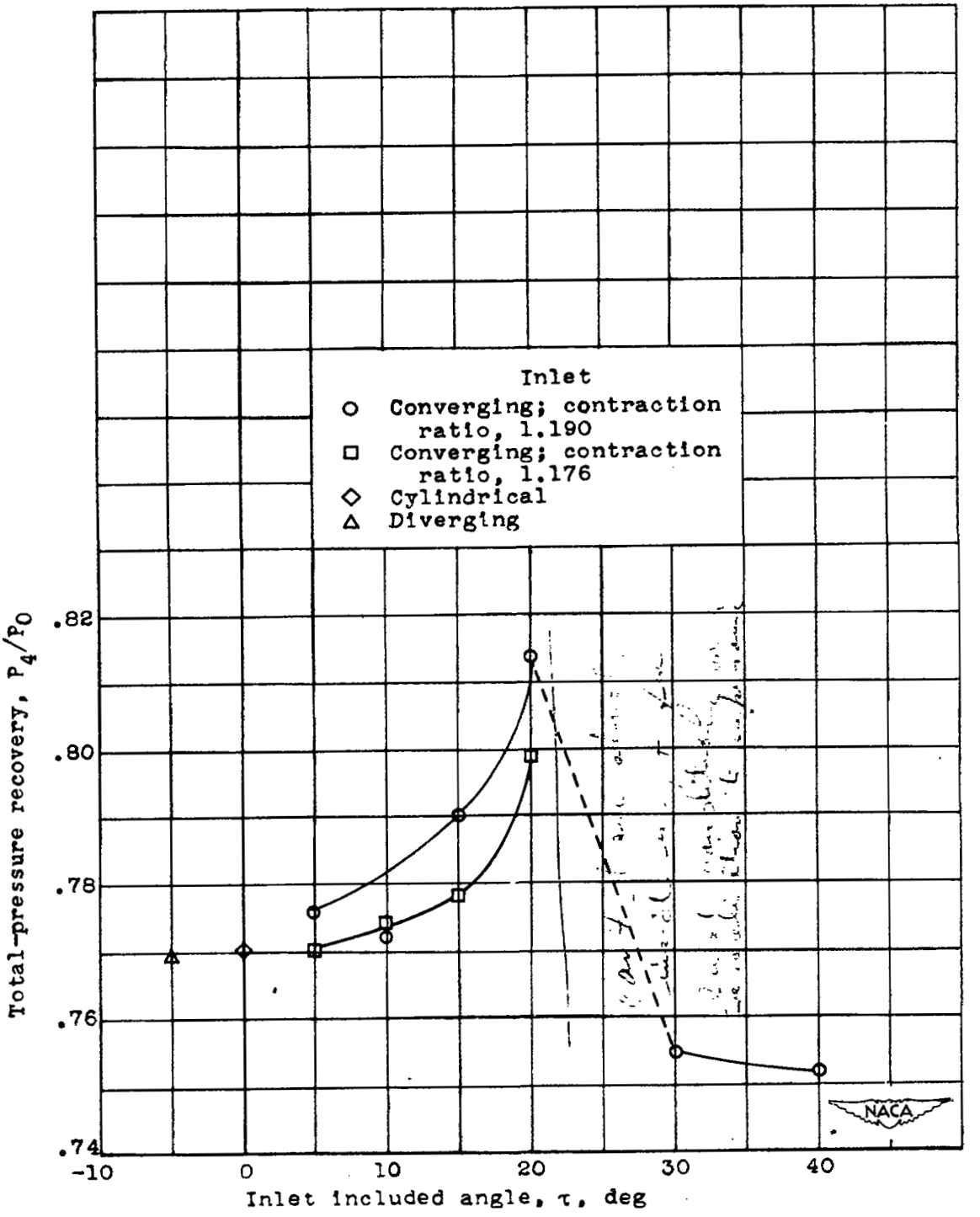

Figure 13.- Effect of inlet angle on maximum total-pressure recovery with normal shock inside diffuser. No throat, angle of attack of 0°.

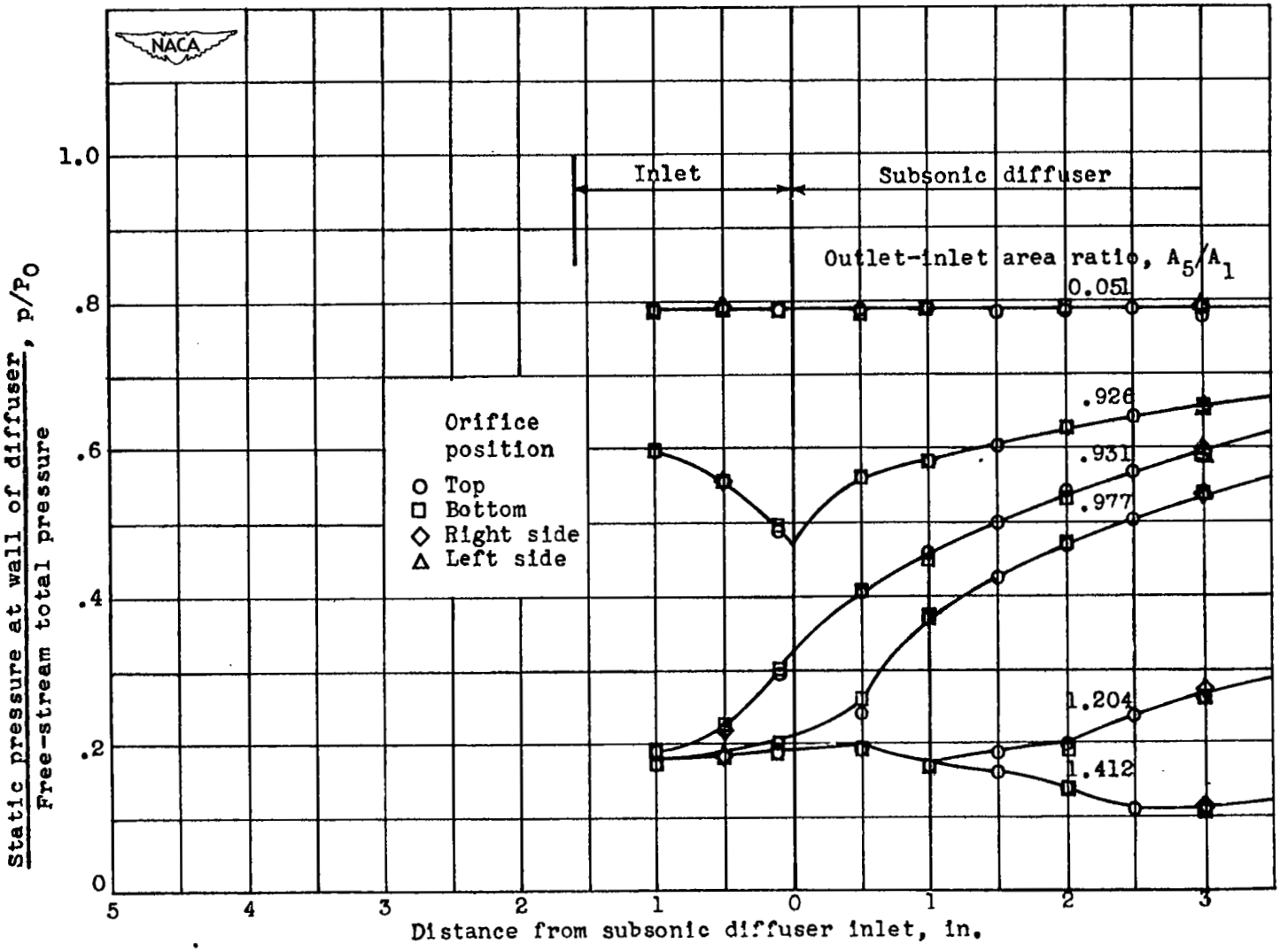

(a) 5-1.176-0 configuration.

Figure 14.- Static-pressure distribution along diffuser for several outlet areas with 5-1.176 inlet at angle of attack of 0°.

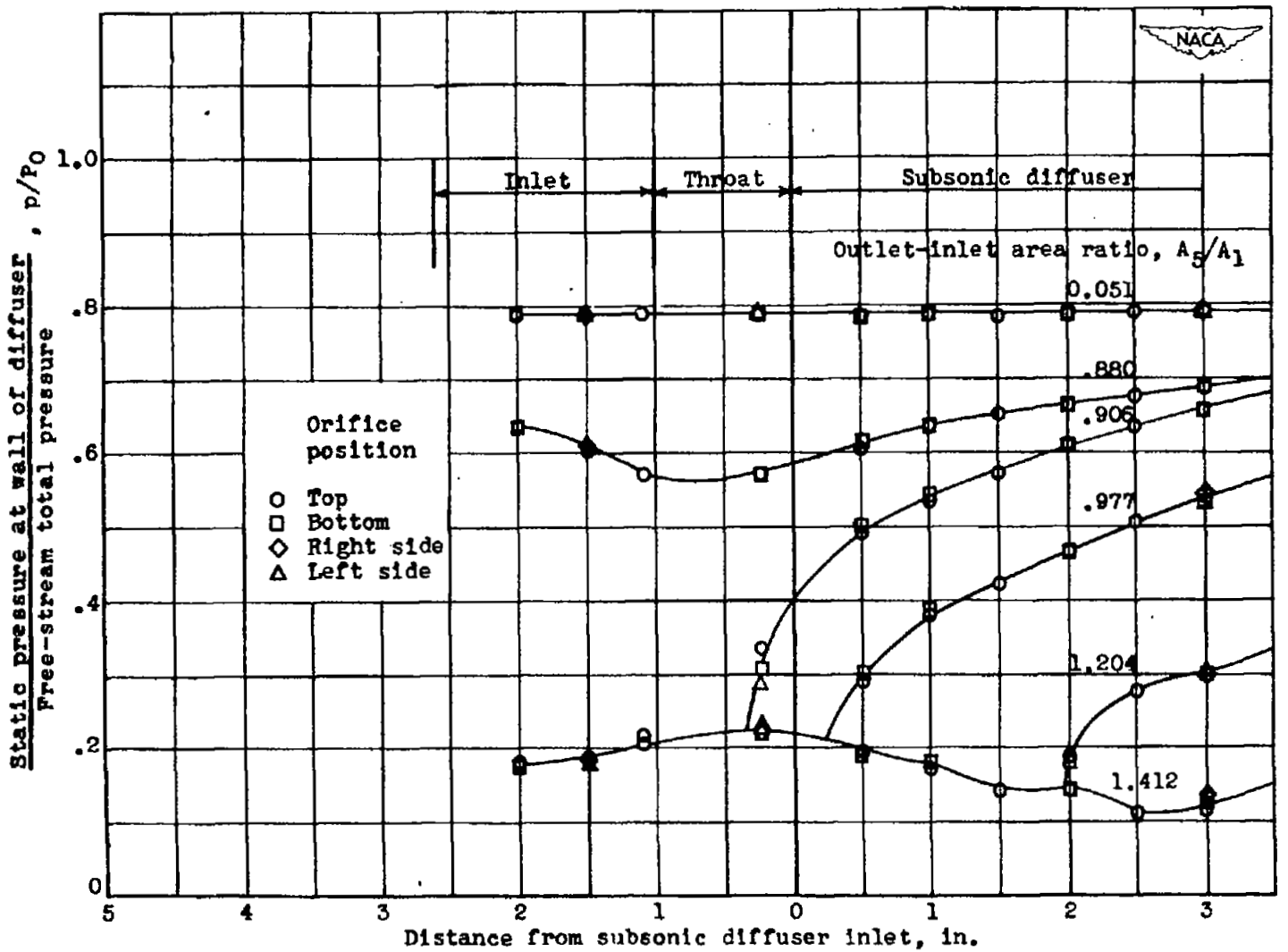

(b) 5-1.176-1 configuration.

Figure 14.- Continued. Static-pressure distribution along diffuser for several outlet areas with 5-1.176 inlet at angle of attack of 0°.

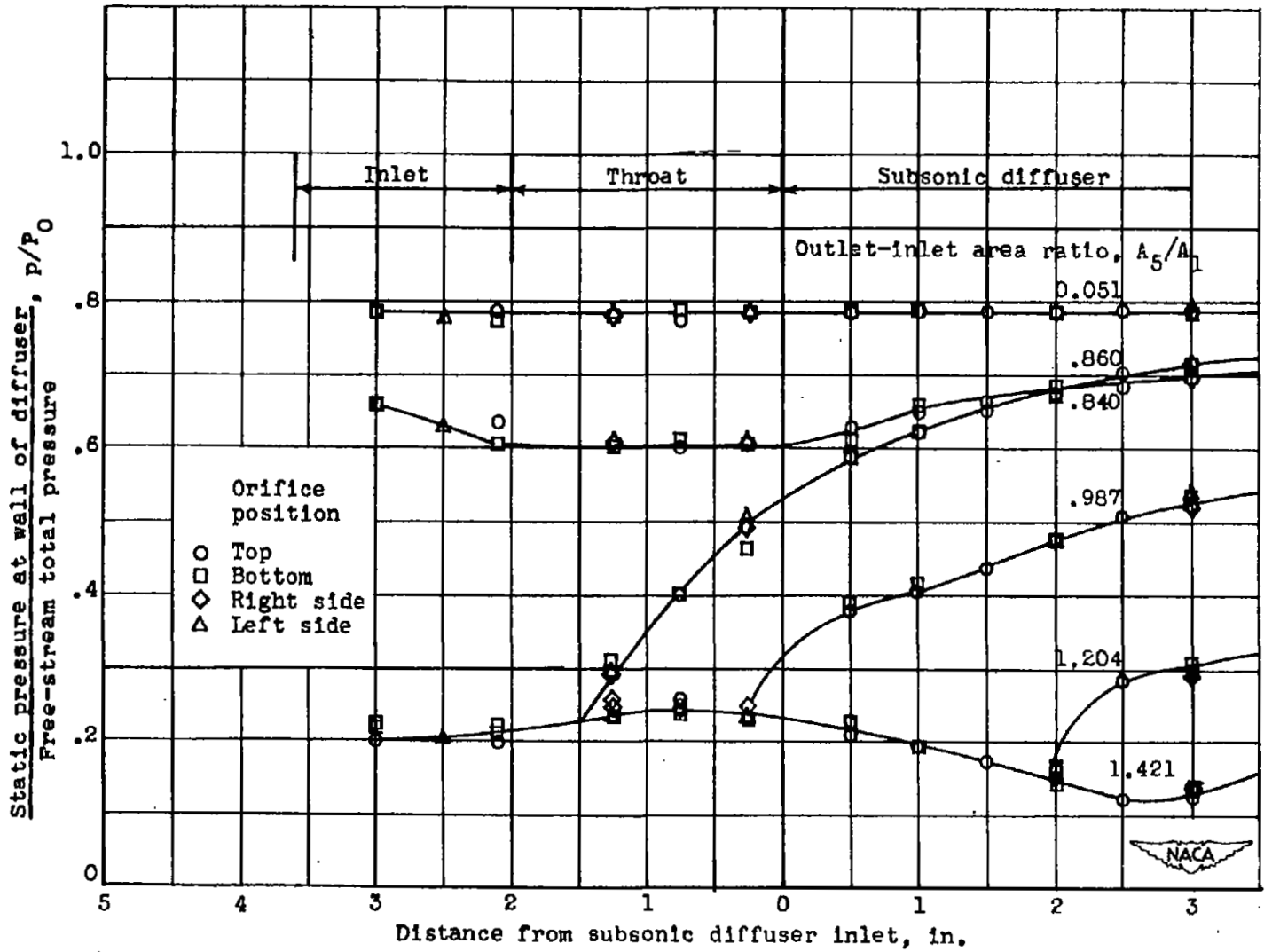

(c) 5-1.176-2 configuration.

Figure 14.- Continued. Static-pressure distribution along diffuser for several outlet areas with 5-1.176 inlet at angle of attack of 0°.

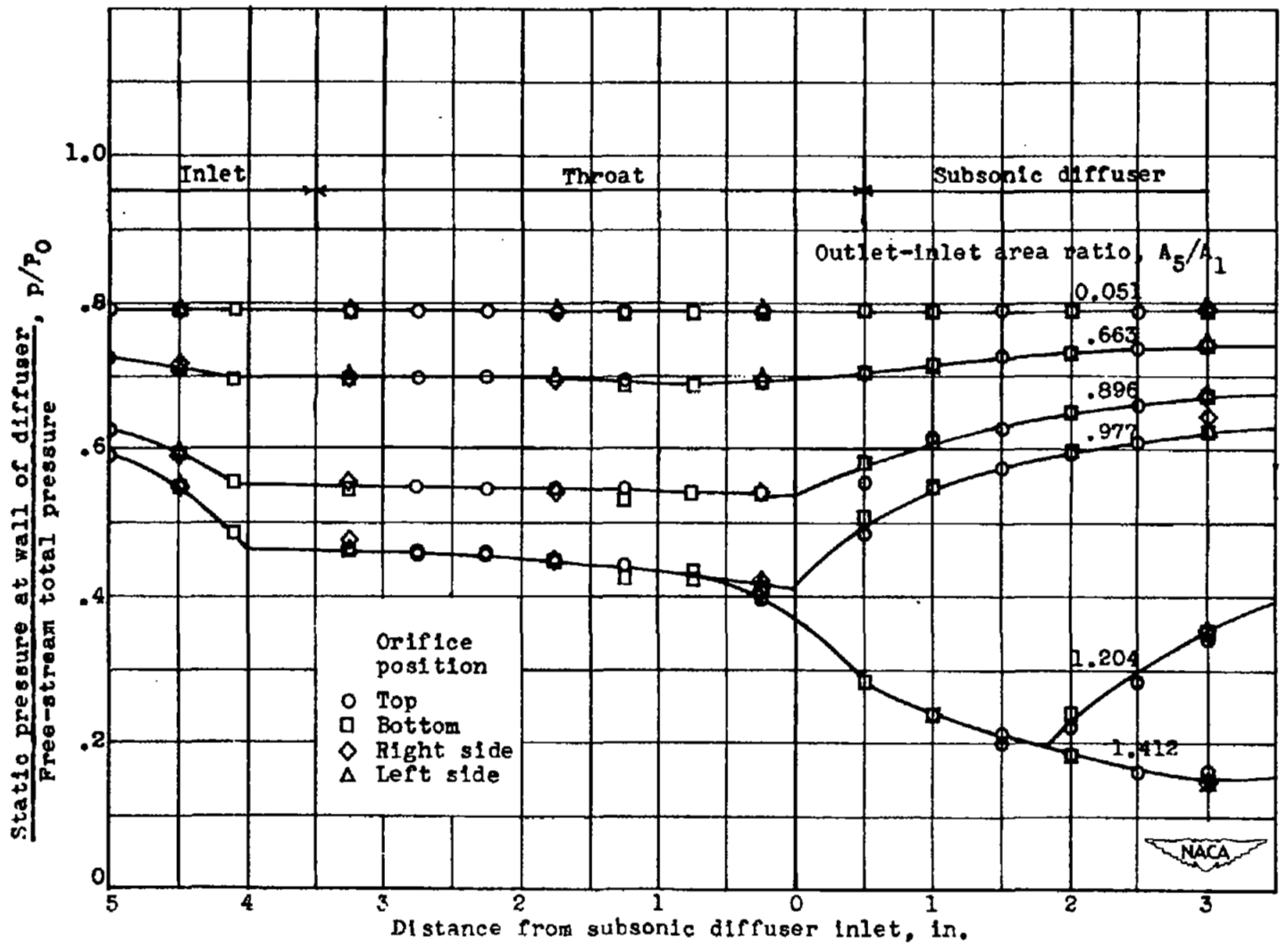

(d) 5-1.176-4 configuration.

Figure 14.- Concluded. Static-pressure distribution along diffuser for several outlet areas with 5-1.176 inlet at angle of attack of 0°.

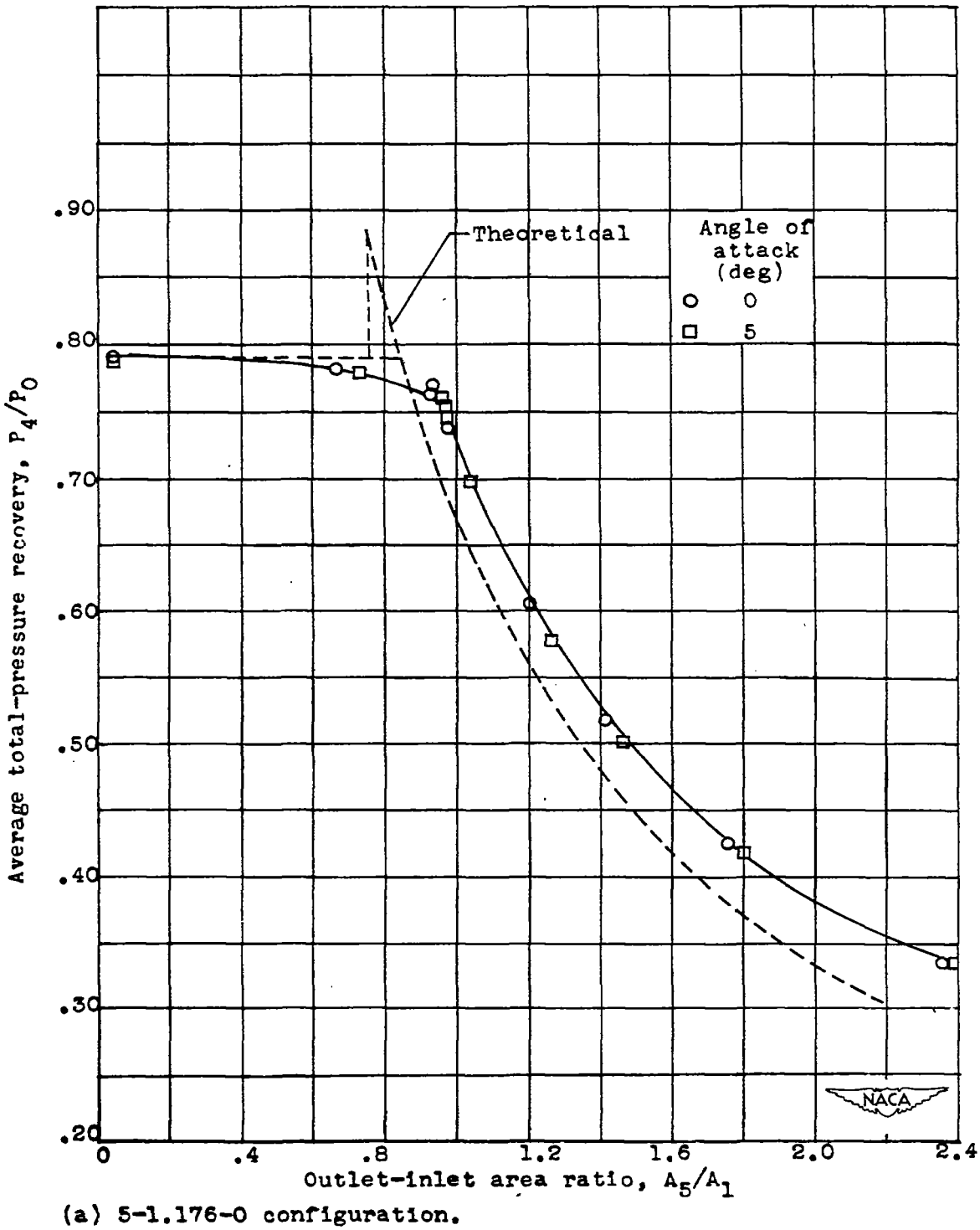

(a) 5-1.176-0 configuration.

Figure 15.- Effect of combustion-chamber-outlet area on average total-pressure recovery with 5 -1.176 inlet.

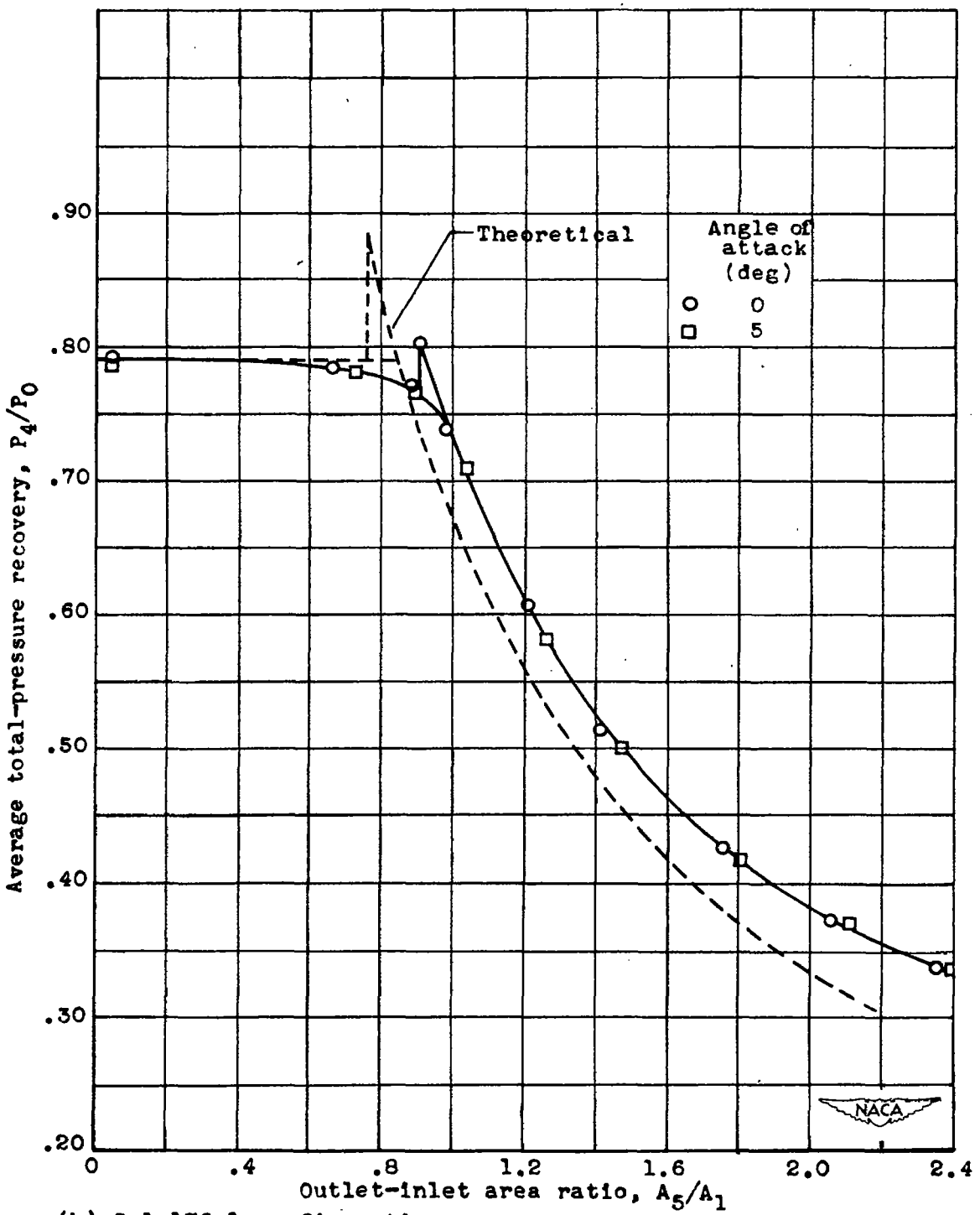

(b) 5-1.176-1 configuration.

Figure 15.- Continued. Effect of combustion-chamber-outlet area on average total-pressure recovery with 5 -1.176 inlet.

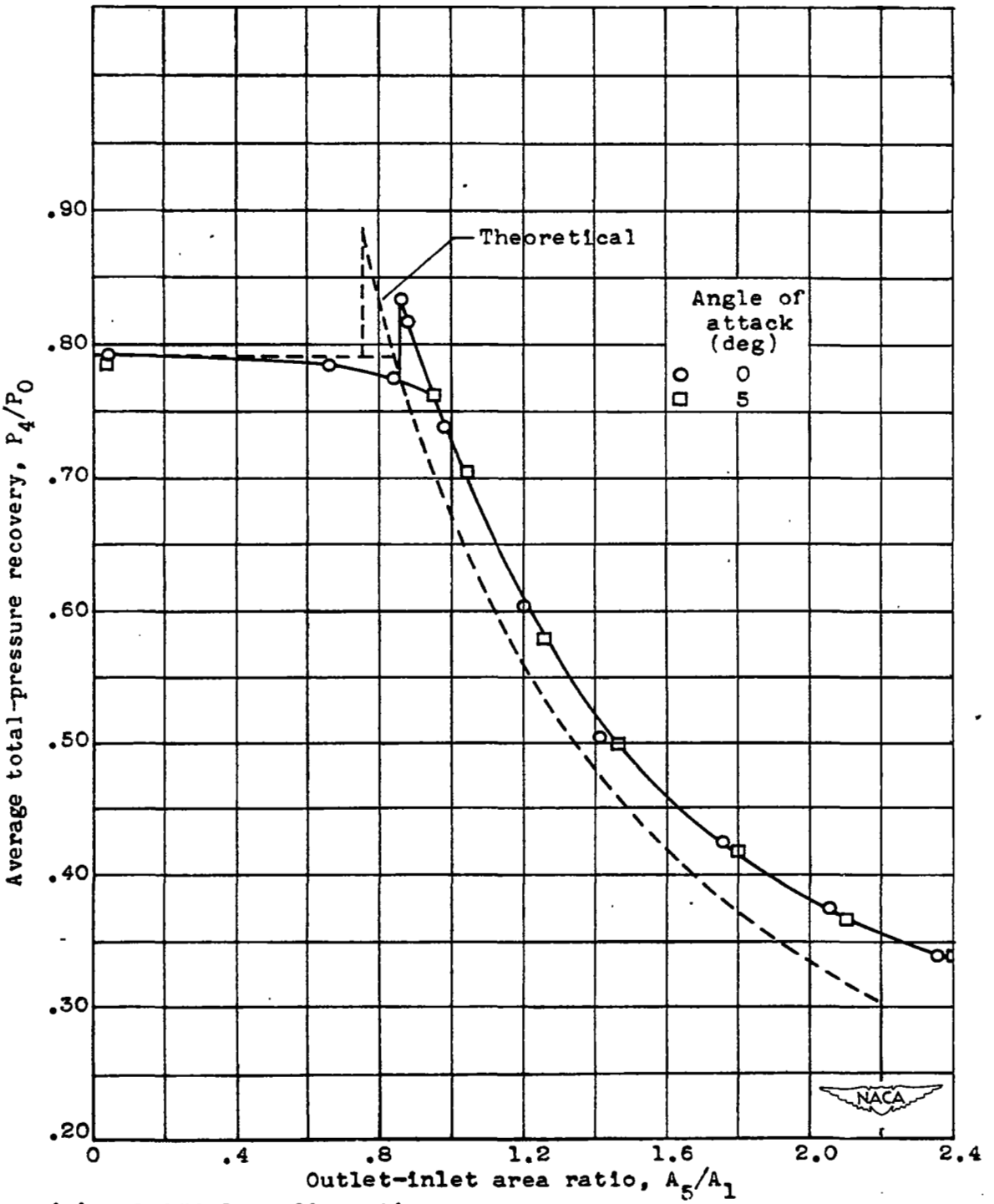

(c) 5-1.176-2 configuration.

Figure 15.- Continued. Effect of combustion-chamber-outlet area on average total-pressure recovery with 5 -1.176 inlet.

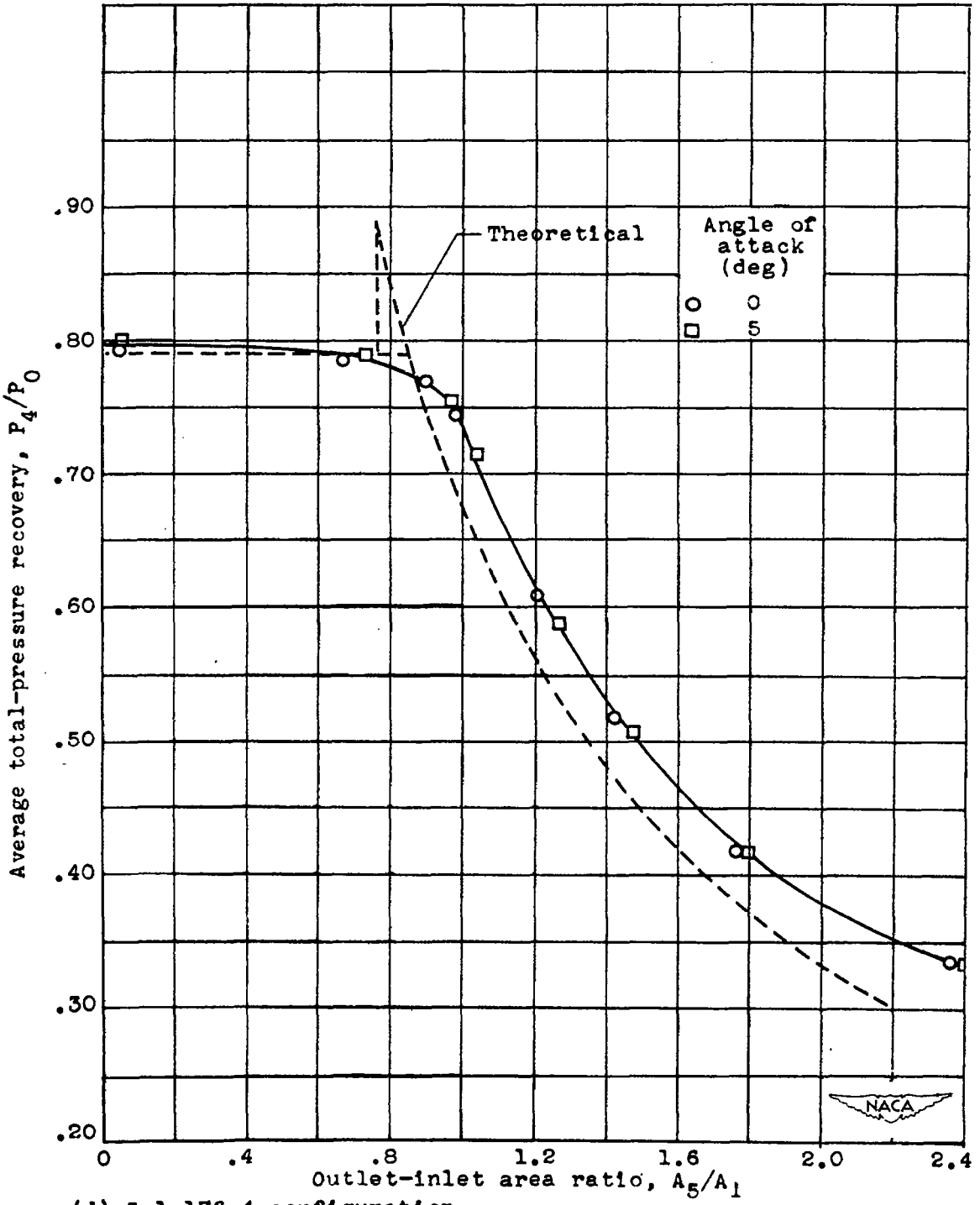

(d) 5-1.176-4 configuration.

Figure 15.- Concluded. Effect of combustion-chamber-outlet area on average total-pressure recovery with 5-1.176 inlet.

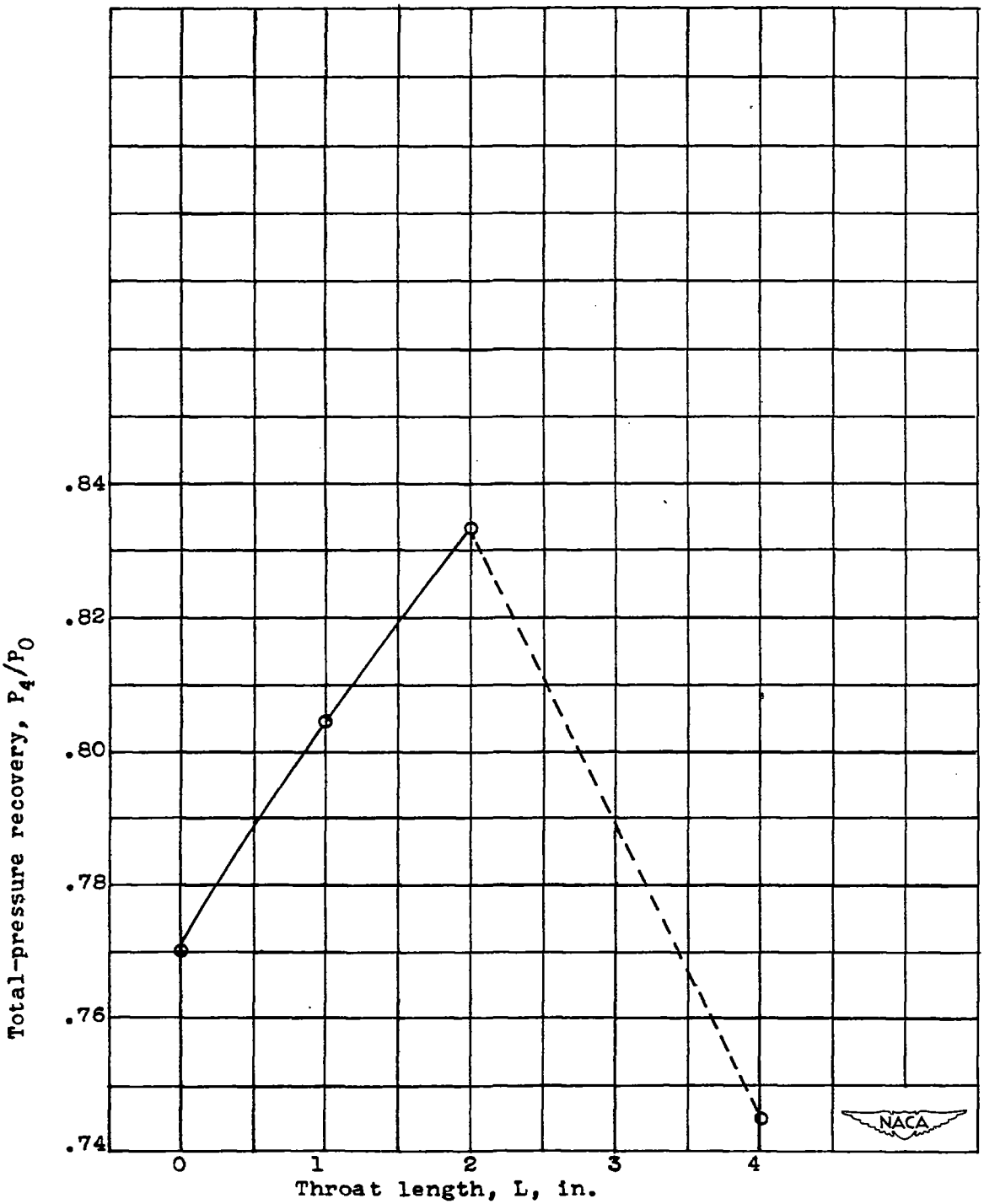

Figure 16.- Effect of throat length on maximum total-pressure recovery with normal shock inside diffuser. 5 -1.176 inlet, angle of attack of 0°.

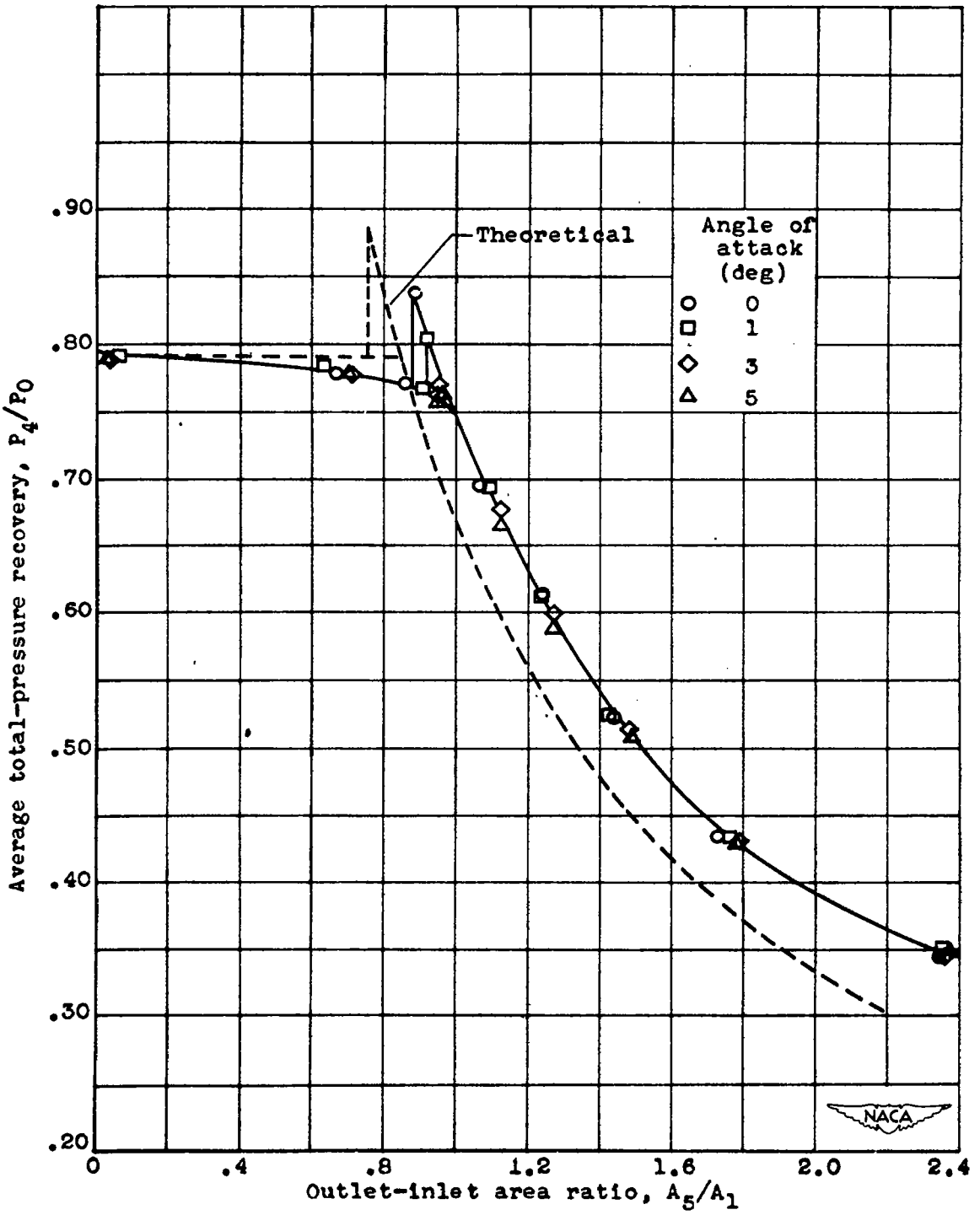

(a) 10-1.176-2 configuration.

Figure 17.- Effect of combustion-chamber-outlet area on average total-pressure recovery with 2-inch throat.

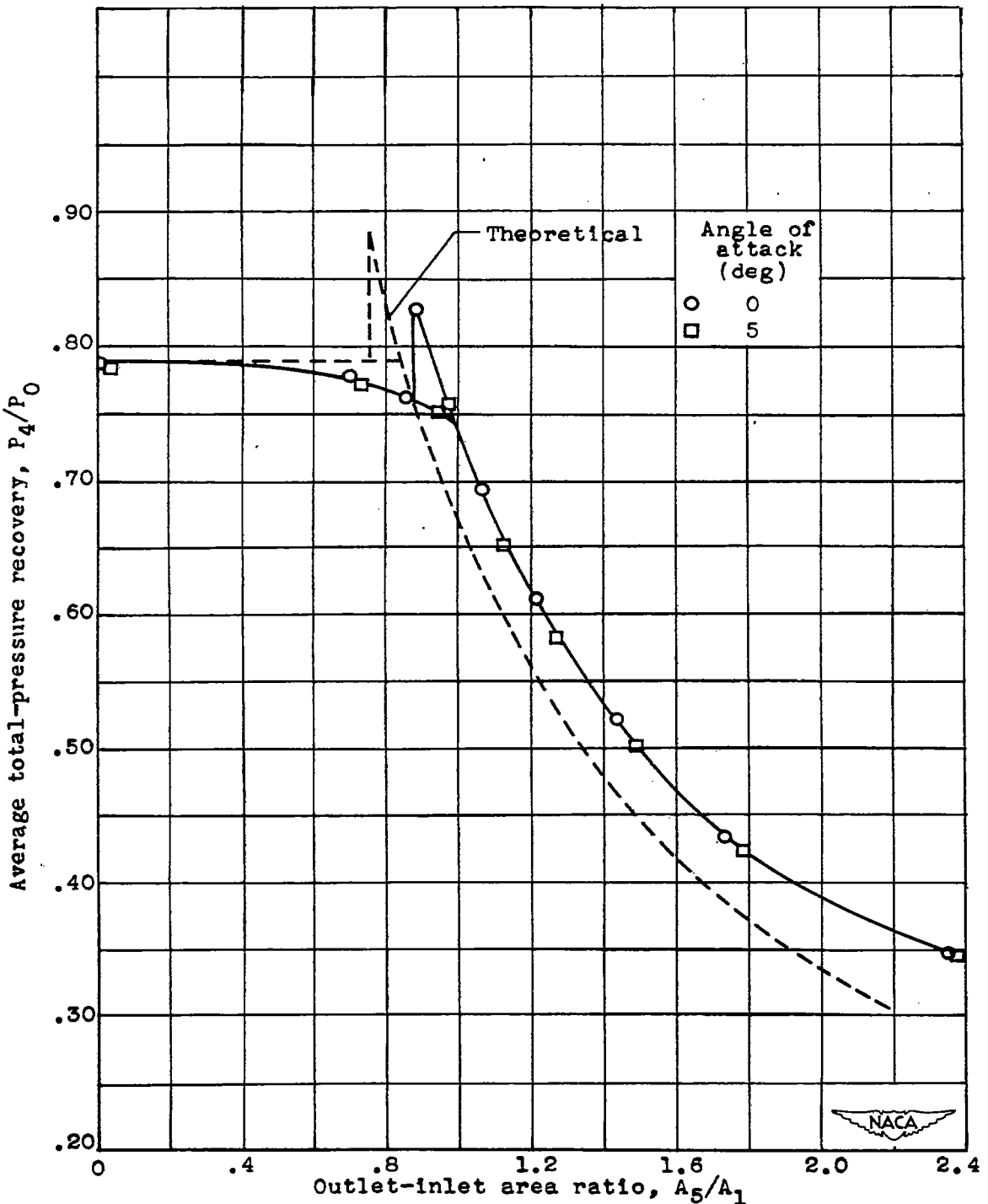

(b) 15-1.176-2 configuration.

Figure 17.- Continued. Effect of combustion-chamber-outlet area on average total-pressure recovery with 2-inch throat.

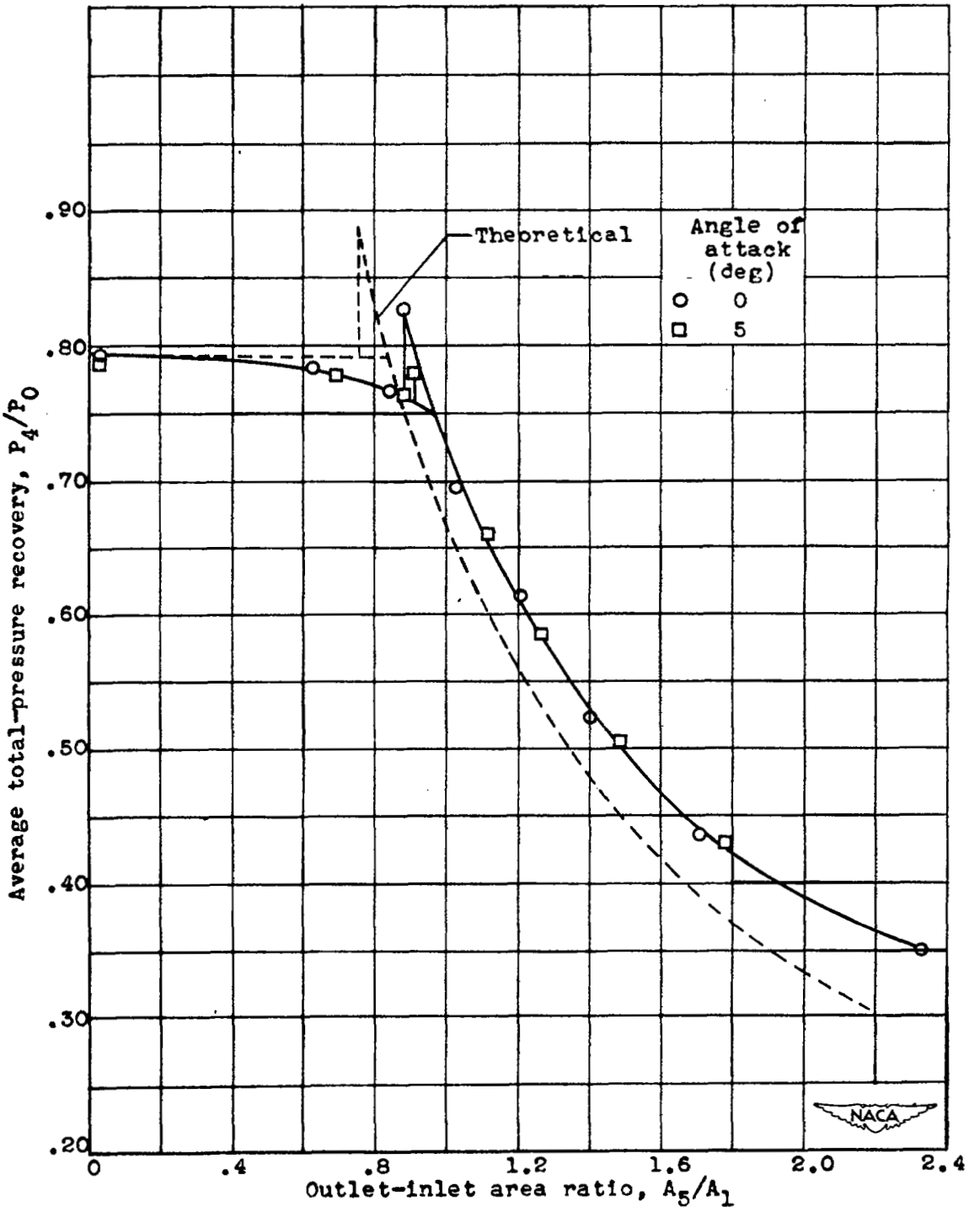

(c) 20-1.176-2 configuration.

Figure 17.- Continued. Effect of combustion-chamber-outlet area on average total-pressure recovery with 2-inch throat.

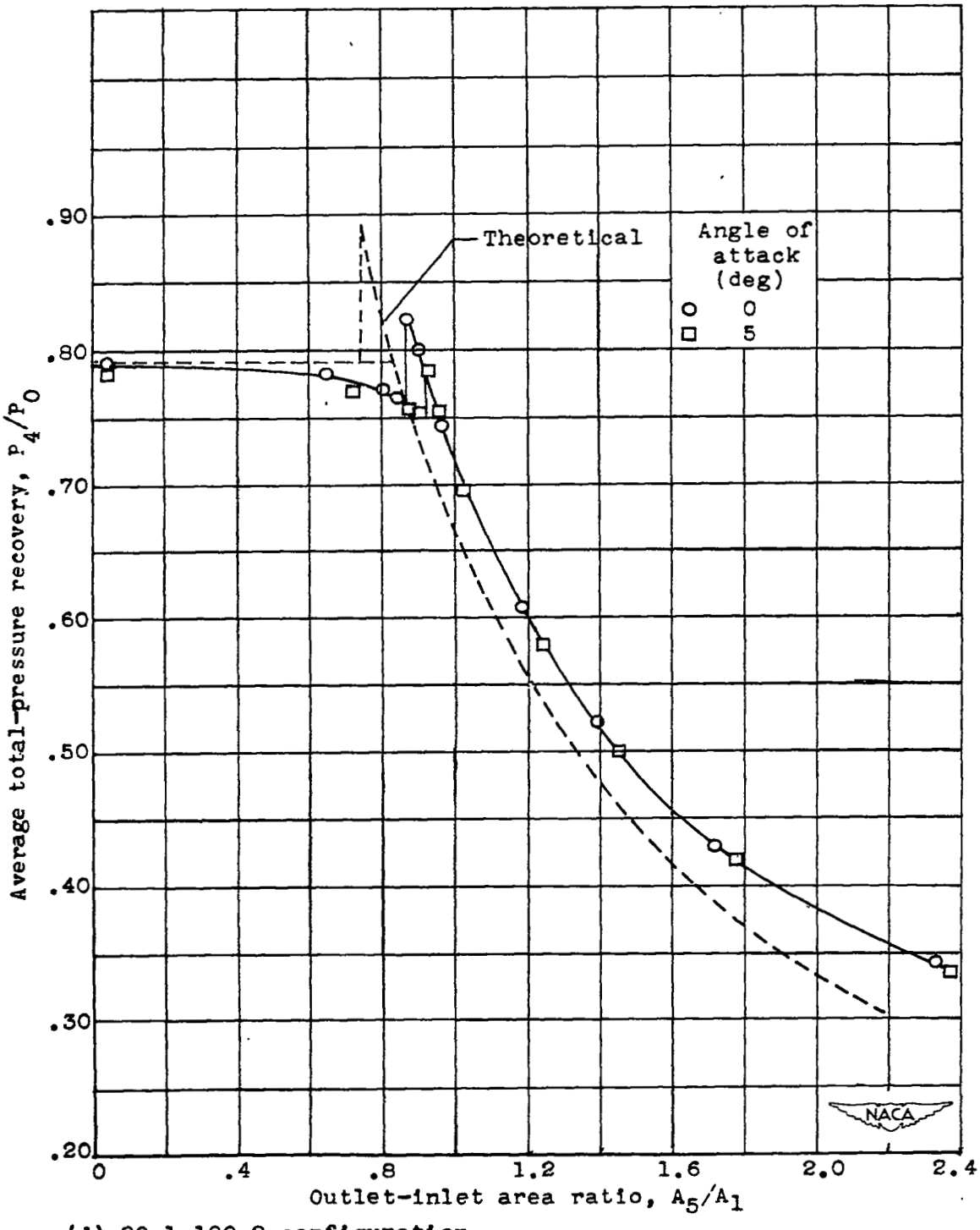

(d) 20-1.190-2 configuration.

Figure 17.- Concluded. Effect of combustion-chamber-outlet area on average total-pressure recovery with 2-inch throat.

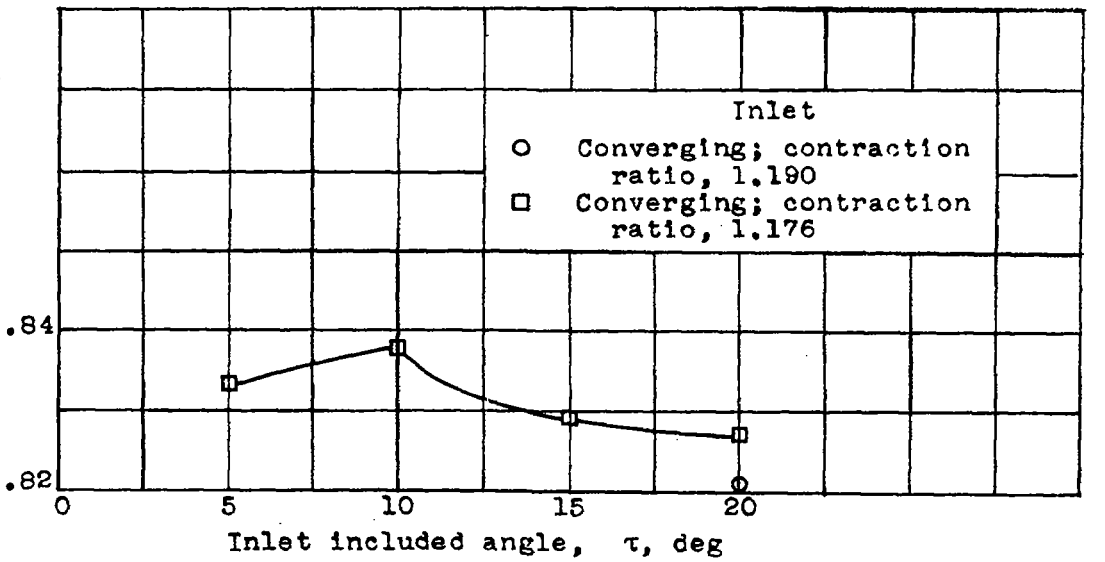

Figure 18.- Effect of inlet angle on maximum total-pressure recovery with normal shock inside diffuser. 2-inch throat, angle of attack of 0°.

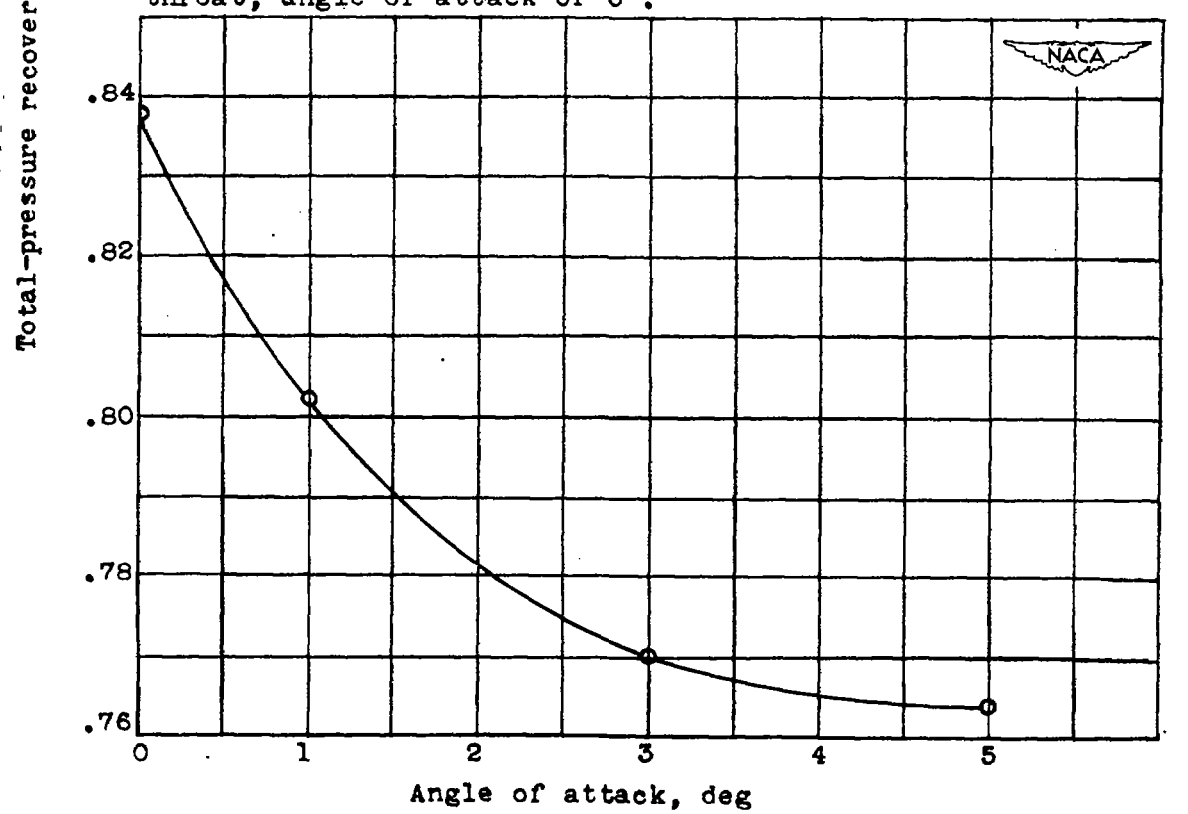

Figure 19.- Effect of angle of attack on maximum total-pressure recovery with normal shock inside diffuser. 10-1.176-0 configuration.

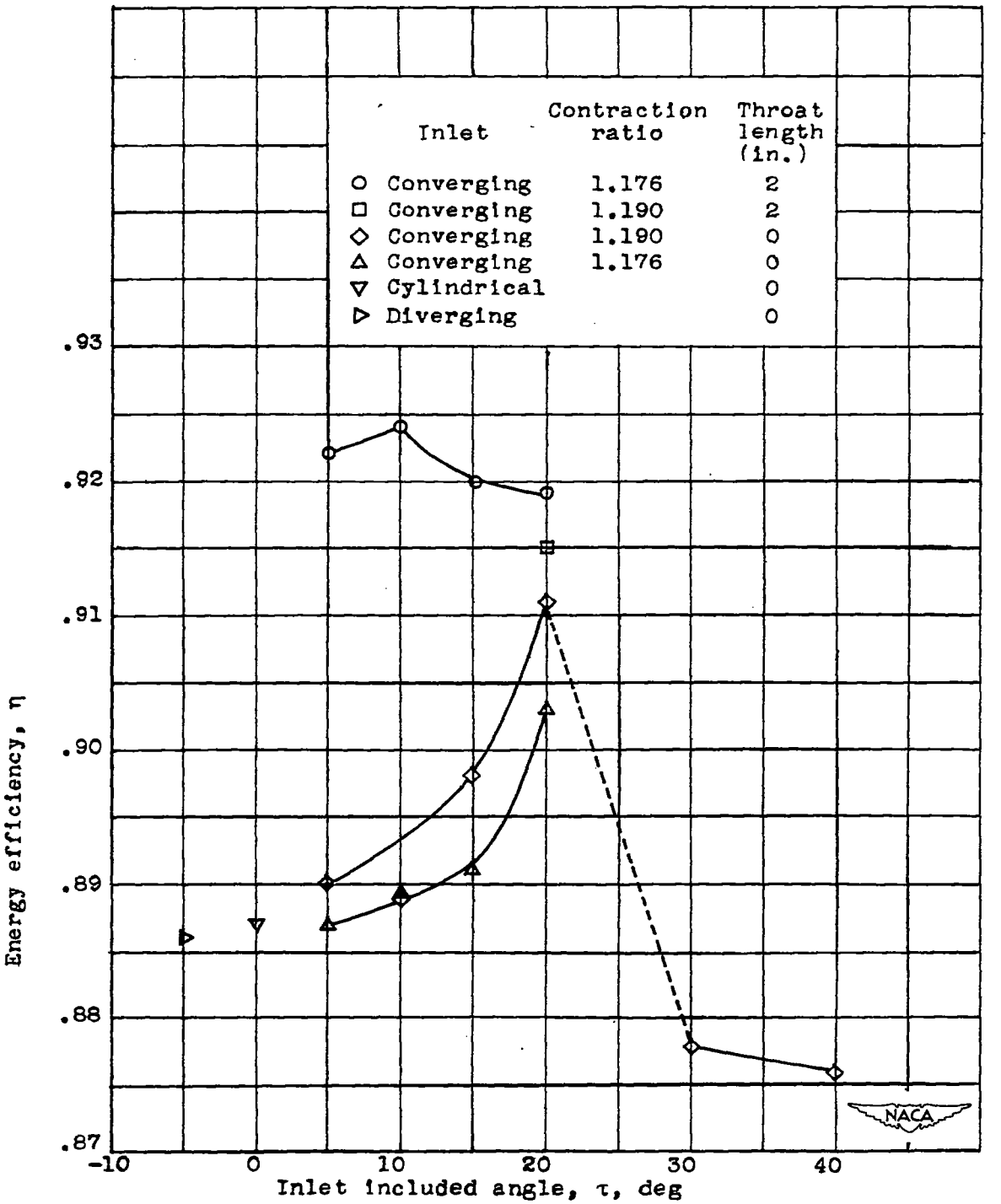

Figure 20.- Effect of inlet angle and throat length on maximum energy efficiency with normal shock inside of diffuser. Angle of attack of 0°.

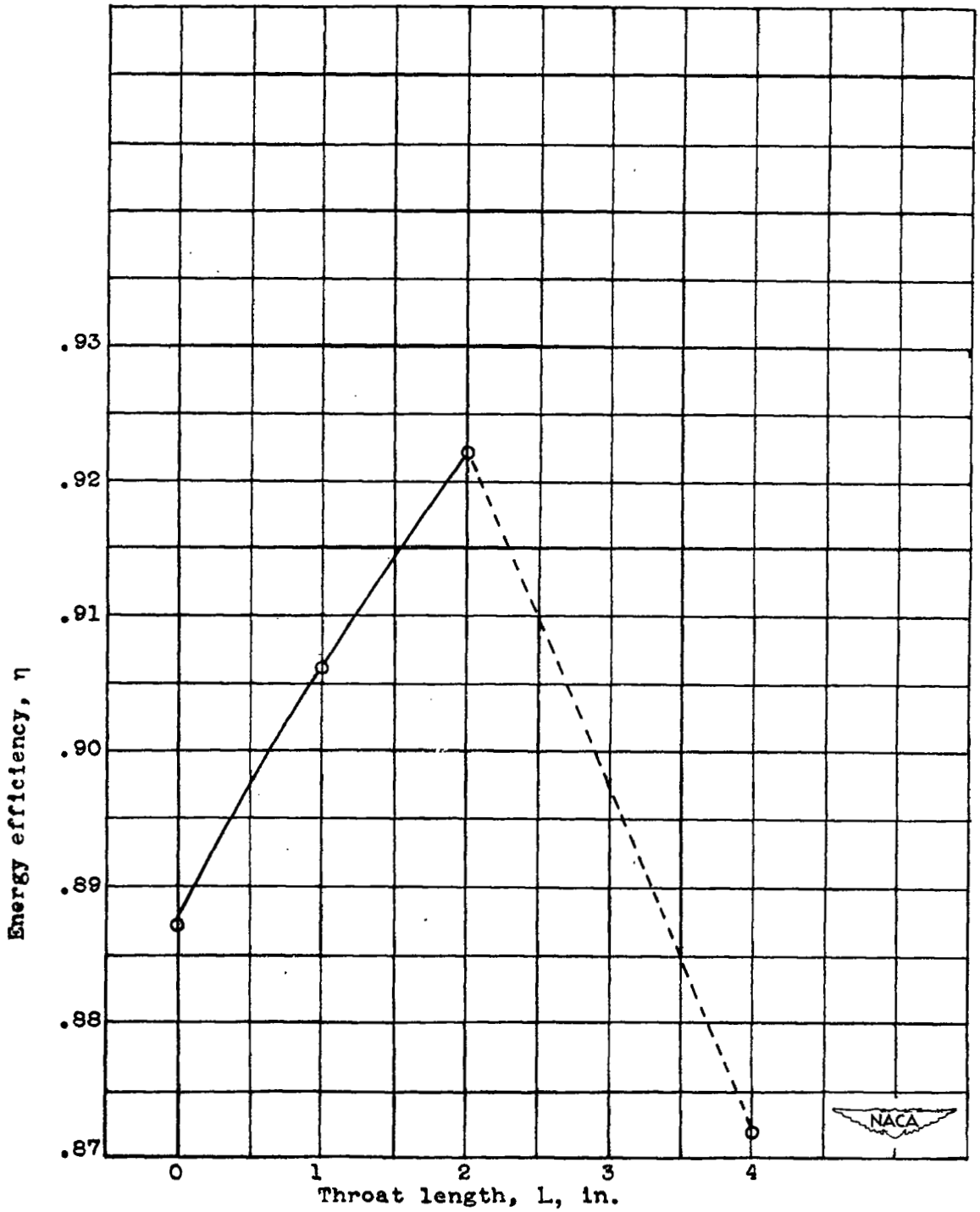

Figure 21.- Effect of throat length on maximum energy efficiency with normal shock inside diffuser. 5—1.176 inlet, angle of attack of 0°.